

Raman scattering in oriented crystals of para-deuterium and orthohydrogen

Walter N. Hardy*

Science Center, Rockwell International, Thousand Oaks, California 91360
and Department of Physics, University of British Columbia, † Vancouver, B.C., Canada, V6T 1W5

Isaac F. Silvera

Science Center, Rockwell International, Thousand Oaks, California, 91360
and Natuurkundig Laboratorium der Universiteit van Amsterdam, † Amsterdam, The Netherlands

John P. McTague*

Department of Chemistry, ‡ University of California, Los Angeles, California 90024
 (Received 3 March 1975)

An extensive rotational-Raman-scattering study on oriented crystals of high-purity para-deuterium and orthohydrogen is presented. The excitations studied include the one- and two-libron bands ($J = 1 \rightarrow 1$), the $J = 1 \rightarrow 3$ rotors, and the $J = 0 \rightarrow 2$ transitions of the impurity $J = 0$ molecules. The use of oriented crystals has permitted a determination of the single-libron mode symmetries which, together with very good frequency agreement with the most recent anharmonic libron theory, provides a firm experimental basis for the $Pa3$ structure. When corrected for virtual ($J = 3$) processes, the single-libron frequencies yield values for Γ_{eff} of $0.747 \pm 0.019 \text{ cm}^{-1}$ (D_2) and $0.582 \pm 0.017 \text{ cm}^{-1}$ (H_2), which are in generally good agreement with other experimental values. New results on the concentration and temperature dependence of libron frequencies and line shapes are also presented. An analysis of the $J = 0 \rightarrow 2$ and $J = 1 \rightarrow 3$ spectra shows that both excitations are strongly coupled to the librations. This results in substantial modifications of the frequencies expected from simple theories, and in the appearance of extra features, interpreted as libron sidebands. In the case of the $J = 1 \rightarrow 3$ band, linear combinations of polarized spectra obtained from oriented crystals has allowed the separation of previously unresolved lines. Spectra of the various rotational transitions in the disordered phase of both H_2 and D_2 are also presented.

I. INTRODUCTION

In the past ten years there has been extensive theoretical and experimental activity directed at the solid hydrogens (H_2 , HD, D_2), and especially at the ground-state and low-lying rotational excitations of the low-temperature orientationally ordered phase of ortho- H_2 and para- D_2 . Raman scattering is particularly well suited to probe the rotational dynamics of such solids, and in this paper we present results for most of the observable pure rotational Raman transitions in oriented crystals of high-purity para- D_2 and ortho- H_2 .

The relatively slow ortho-para conversion rate provided by nature in solid hydrogen and deuterium (1.9%/h for H_2 , and 0.056%/h in D_2), allow one to prepare and study samples which are in a metastable rotational state, $J=1$. Solids having high concentrations of the $J=1$ species have many properties in common with magnetic systems. In particular, at low temperatures (3.8 K in pure para- D_2 and 2.8 K in pure ortho- H_2) there is an orientational ordering of the $J=1$ molecular orbitals, closely analogous to the spin ordering in an antiferromagnetic system.¹ One of the most challenging problems has been the determination of the ground state of the orientationally ordered

solid, i.e., the space group of the crystal at $T=0$ K. The structure is difficult to determine by the standard techniques, x-ray and neutron diffraction, because in addition to the usual problems encountered in locating protons or deuterons, the diffraction lines associated with the orientational order are weakened by the near sphericity of the molecule, and by the fact that the molecule is in the quantum state $J=1$. [This results in a further reduction in the cross section by $\frac{4}{25}$ (Ref. 2).] X-ray measurements³ had determined that at the transition to the low-temperature phase the molecular centers transformed from an hcp to an fcc lattice, however, the orientations of the molecules could not be determined. Subsequent neutron-diffraction data⁴ were consistent with the $Pa3$ space group predicted theoretically on the basis of a pure electrostatic quadrupole-quadrupole (EQQ) anisotropic intermolecular potential.⁵ However, the validity of these measurements remained in doubt because of strongly interfering background peaks.

In the $Pa3$ structure each molecule sits at an fcc lattice site with the axis of the $m_J=0$ molecular orbital oriented along one of the $[111]$ body diagonals. The arrangement is such that for each of the four simple-cubic sublattices comprising the

fcc structure, the molecular orbitals are parallel. In the molecular-field approximation the ground $m_J=0$ state is separated from the degenerate $m_J=\pm 1$ states by 19Γ , where $\Gamma=6e^2Q^2/25R_0^5$ is the EQQ coupling parameter. (If the lattice sums are extended to all neighbors the splitting becomes 21.2Γ .)

The $m_J=\pm 1$ (or suitable linear combinations) levels correspond to molecular orbitals which are oriented at 90° to the ground $m_J=0$ orbital. However, the elementary reorientational excitations of the solid are not these molecular-field states but rather the librins: spin-wave-like collective excitations¹ within the $J=1$ manifold of states. On the basis of a $Pa3$ structure a number of authors^{6,7} used simple spin-wave theory to calculate the dispersion relations and other properties of the librins. The frequencies of the librins were predicted with rather high precision in terms of the single parameter Γ , whose value in the solid was also presumed to be well known. They give eight modes for general \vec{k} , and three distinct frequencies at $k=0$. We realized that these $k=0$ modes should be Raman active and identified them by their group-theoretical labels as E_g , $T_g^{(1)}$, and $T_g^{(2)}$ which are twofold, threefold and threefold degenerate, respectively. In our original Raman experiments,⁸ at least four distinct features were observed in the region of the expected libron bands ($\sim 5-15 \text{ cm}^{-1}$) in polycrystalline samples of both ortho- H_2 and para- D_2 . The three lower-frequency features were much sharper than the highest-frequency feature. Not only was an extra feature observed, but the three lowest lines were substantially lower in frequency than expected from theory, and simple scaling of $\Gamma \equiv \Gamma_{\text{eff}}$ was inadequate to identify the lines by means of a frequency fit. Two possible models were proposed to explain the observations: (i) The three lower-frequency lines were the single-libron transitions with the fourth being a two-libron transition; and (ii) the actual structure was distorted from $Pa3$ in such a way that the degeneracy of the single-libron model was partially lifted, explaining the extra feature. Although the first model yielded reasonable intensities, the frequencies were in serious disagreement with theory, whereas this was apparently not a problem in the second model.

A number of attempts to explain the observations were made. An extension of the range of the EQQ interaction from nearest-neighbors only to a sum over all neighbors⁹ was inadequate as it could be represented by a new value of Γ_{eff} . Likewise, consideration of the effects of the large zero-point motion in the hydrogen lattice led to a renormalized Γ_{eff} .¹⁰ We obtained new and improved Raman data,¹¹ still on polycrystalline samples, in which

the $J=0 \rightarrow 2$ spectra of $J=0$ species in the $J=1$ solids were observed. This provided information about the local-site symmetry of the ordered solid and essentially eliminated the proposed distortion of the $Pa3$ structure. A number of possible metastable structures (all less favorable than $Pa3$) were predicted by James.¹² Coll and Harris¹³ considered one of these structures but were unable to obtain a fit of libron frequencies to experiment, although a good frequency fit to the distorted $Pa3$ structure could be obtained if non-EQQ anisotropic terms were added to the interaction potential. Nakamura and Miyagi¹⁴ then calculated the frequencies for the three single-libron plus two-libron model, but there still remained a serious problem with the frequency fit, and the mechanism they provided for the two-libron line was unable to account for the observed intensity. Coll *et al.*^{15,16} then realized that cubic anharmonic terms of the EQQ Hamiltonian were very important and on the basis of diagrammatic perturbation theory were not only able to provide a good frequency fit for the undistorted $Pa3$ structure based on a single parameter Γ_{eff} , but were also able to explain the intensity and structure of the two-libron feature.¹⁷ At this same time we succeeded in growing oriented crystals of ordered H_2 and D_2 . The polarized Raman spectra of these samples allowed a definite identification of the three lower-frequency modes as the single-libron modes of the undistorted $Pa3$ structure.¹⁸ Recently, a new elastic-neutron-scattering study by Mills *et al.*² has provided further, direct proof of the $Pa3$ structure.

In spite of the good agreement between theory and experiment for the Raman observed lines, there remained a variance in the value of Γ_{eff} measured by different experimental techniques, especially for D_2 . Recently, Harris *et al.*¹⁹ have shown that this could be largely accounted for by mixing of the $J=3$ state into the ground $J=1$ state (virtual $J=3$ processes), an effect which is larger for D_2 because of the smaller splitting between the $J=1$ and 3 rotational levels. A substantial part of the present paper is concerned with a detailed presentation of the earlier reported¹⁸ libron spectra in oriented crystals, and an analysis in terms of the latest theoretical refinements.

In addition, previously unpublished data of the dependence of libron frequencies on $J=1$ concentration, two-libron spectra, libron line shape, and the temperature dependence of the libron linewidth are presented. The temperature dependence of libron frequencies has also been studied. In the random-phase approximation (RPA), this dependence should be that of the orientational order parameter $\langle 3J_z^2 - J(J+1) \rangle$. The temperature dependence compares reasonably with theoretical

and experimental curves of the order parameter versus temperature.

At this point it is useful to make a critique of some of the experimental methods used to study the librions. The thermodynamic measurements, such as specific heat and $(\partial P/\partial T)_V$,²⁰ provide information about the ordering—long and short range—and the size of the interaction; however, the information is in the form of thermodynamic averages over density-of-states functions and is not sensitive to the details of the structure and dynamics of the ordered state. Likewise, NMR, although very useful in measuring the temperature dependence of the order parameter,²¹ is also insensitive to much of the detail. The ideal set of measurements for studying the structure and dynamics would be elastic and coherent inelastic neutron scattering, the former to determine the structure and the latter the dispersion relations of the librions, i.e., the low-energy states of the solid as a function of wave vector. Unfortunately, the experimental problems are severe and the possibility of the latter study still seems remote. (Incoherent neutron scattering has been analyzed to determine the libron density of states.²²) Optical measurements, which do not suffer from many of the experimental restrictions of neutron scattering also can be used to obtain detailed information concerning the energy states of the solid, although limited to certain regions of the Brillouin zone. In fact, this restriction to $\vec{k}=0$ was initially an advantage in the study of the ordered state since it simplified the interpretation of the rather surprising spectra that were observed. The observation of librions as sidebands or combination bands in infrared²³ and Raman spectroscopy, although providing detailed energy information, still involves excitations throughout the Brillouin zone which substantially increases the complexity of sorting out the spectra and in some cases, the difficulty of distinguishing between pure first-order or combination spectra. These problems are also present in the interpretation of the $\Delta J \neq 0$ Raman rotational transitions where the librions apparently occur as sidebands.

In this paper we also present new measurements of the Raman spectra associated with $J=0 \rightarrow 2$ impurity transitions²⁴ and $\Delta J=1 \rightarrow 3$ roton bands.^{8,24} The nominally pure $J=1$ solid always contains $J=0$ impurity species due to either incomplete initial separation or to conversion. For low $J=0$ concentration the impurity sits in a $J=1$ environment. The Raman selection rules $J=0, \pm 2$ allow transitions to the $(2J+1=5)$ $J=2$ states, whose degeneracy is partially lifted by the interaction of the EQQ moment in the $J=2$ state with the electric-field gradient from the ordered sur-

rounding $J=1$ molecules. One might expect to be able to predict the line splittings reasonably well with a molecular-field theory. For the $Pa3$ structure the number of distinct lines should be three because of the local point symmetry (C_{3i}) and the number of symmetry-inequivalent sites (one). The observed spectrum of four features, none of which correspond to molecular-field-theory predictions, is interpreted as being composed of the three impurity transitions plus libron sidebands, the interaction with the libron probably resulting in large energy shifts from the molecular-field predictions.

Similarly unusual results are found for the $J=1 \rightarrow 3$ bands. Because the $J=3$ excitation can occupy any lattice site of the pure $J=1$ solid there are exciton bands which for any value of the wave vector \vec{k} have a multiplicity of 28 due to the four symmetry-equivalent sites and the $2J+1=7$ states per site. The degeneracy is partially removed by anisotropic interactions. The earlier spectra^{8,24} showed an unexpectedly small number of distinct features. In the present work we have processed the polarized spectra from oriented crystals to show that the features actually consist of several overlapping unresolved lines. The spectra, which disagree with simple spin-wave theory, are interpreted as both pure $J=3$ roton, and roton-libron combination bands.

The paper is organized as follows. In Sec. II we discuss experimental techniques; Sec. III is devoted to the libron spectra. The $J=0 \rightarrow 2$ impurity spectra and $J=1 \rightarrow 3$ roton bands are considered in Sec. IV, measurements of ortho-para ratio and conversion rate are presented in Sec. V, followed by a general discussion in Sec. VI. The paper is concluded with an appendix on Raman intensities and on the data-processing techniques employed in analyzing the $J=1 \rightarrow 3$ spectra.

II. EXPERIMENTAL TECHNIQUES

A. Preparation of ortho-para species

Samples of *o*-H₂ and *p*-D₂ were prepared from normal gas using an absorption column of the type described by Depatie and Mills.²⁵ For this method it is necessary to maintain a long column of activated alumina at a temperature of about 20 K. This is most easily achieved with a liquid-hydrogen bath. In order to minimize the amount of liquid hydrogen brought into the laboratory (for safety considerations) a special cryostat was designed and is shown in Fig. 1. The system couples a long insulated tube to a small 2½ liter storage Dewar. By pressurizing the liquid hydrogen in the Dewar the hydrogen level could be raised to the top of the cryostat. The required pressure was maintained with a manostat, which

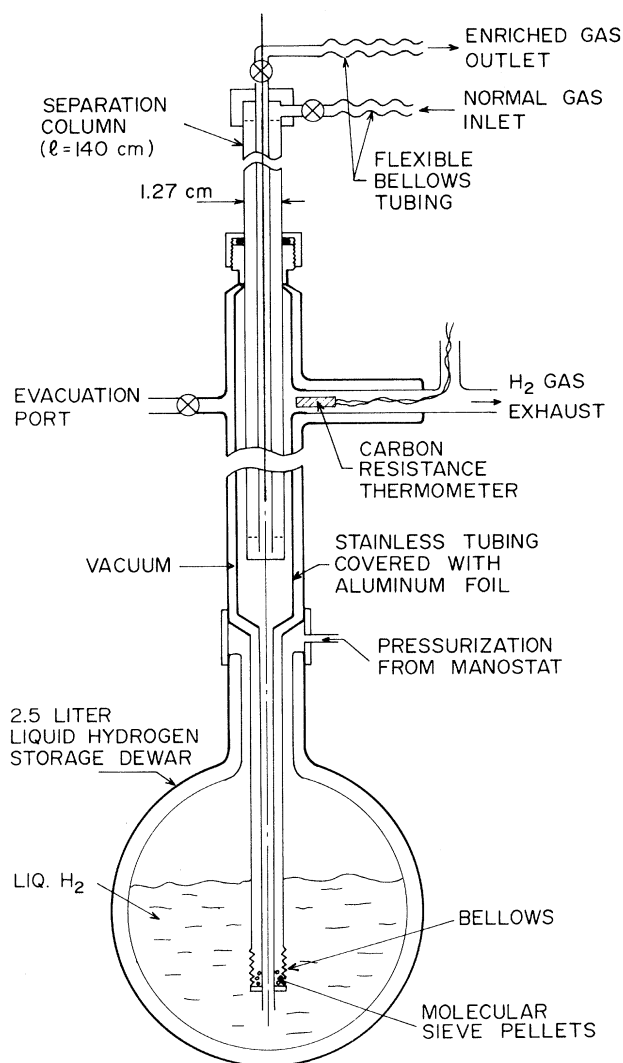


FIG. 1. Cryostat used in ortho-para separation. The separation column, which is packed with activated alumina, is cooled by forcing the liquid hydrogen up the center tube to the desired level.

was set by monitoring the liquid level with a carbon resistance thermometer. Desorption was achieved by withdrawing the column from the cryostat at a fixed rate of about 4 cm/min. (The optimum rate depends on the unavoidable ortho-para conversion taking place on the surface of the alumina, and differs for H_2 and D_2 .)

To obtain reasonable quantities of high-purity gas per desorption it was necessary to experiment with the activation procedure for the alumina in the column. The efficiency of the separation in which the odd J species is preferentially adsorbed, is limited by the rate of conversion of the $J=1$ to $J=0$ species on the alumina. It was found that prolonged heating of the alumina in a vacuum to

temperatures greater than $200^\circ C$ caused the low-temperature conversion rate to be considerably increased, thereby reducing the efficiency of the separation column. The activation procedure finally adopted was to heat to $100^\circ C$ under vacuum for 1 day. (Overheated alumina could be at least partly restored to its original condition by exposure to air for a day or so.) In an attempt to further reduce the ortho-para conversion rate, the alumina (Alcoa grade F-1) was thoroughly washed before activation with concentrated HCl to remove certain paramagnetic impurities, mainly Fe^{+++} ; however, no definite proof of the efficacy of this procedure was obtained.

The initial purities of the gases used were 99.999% for hydrogen (Matheson ultra-high purity), and 99.65 at.% for deuterium (Bio-Rad laboratories). The yield per desorption run was about 2 liters at NTP with odd- J concentration $\sim 99\%$ for $p-D_2$ and $\geq 99\%$ for ortho- H_2 . Samples were stored at approximately 1-atm pressure in baked-out Pyrex bulbs. Deuterium samples could be stored for periods of order weeks without noticeable degradation in purity. Samples of hydrogen, however, converted more quickly and had to be used within a few days if the highest purity was to be achieved.

Subsequent handling of the gas samples undoubtedly introduced impurities such as out-gassing products from parts of the vacuum system that could not be heated, and in some cases small quantities of air. However, the fact that the crystals were grown slowly from the liquid ensured that the concentrations of molecules in solid solution were close to that given by the equilibrium solubilities at temperatures below the melting point. For non-hydrogen impurities these solubilities are extremely low at the partial pressures involved.²⁶

B. Crystal growth

The key to the present series of experiments was the ability to obtain optically clear single crystals with known orientation for all of the species of hydrogen and deuterium. For para-deuterium and orthohydrogen it was also important that crystal growth take place fairly quickly because of the finite rate of ortho-para conversion ($\sim 1.9\%/h$ for solid H_2 and $0.06\%/h$ for solid D_2). The growth techniques were similar to those outlined previously.¹¹ The samples were first rapidly solidified by lowering the Raman cell (a 1.2-cm-diam Pyrex tube) into the liquid helium, at which point the valve to the sample bulb was closed (Fig. 2). The cell was then lifted above the liquid helium, the sample remelted with the

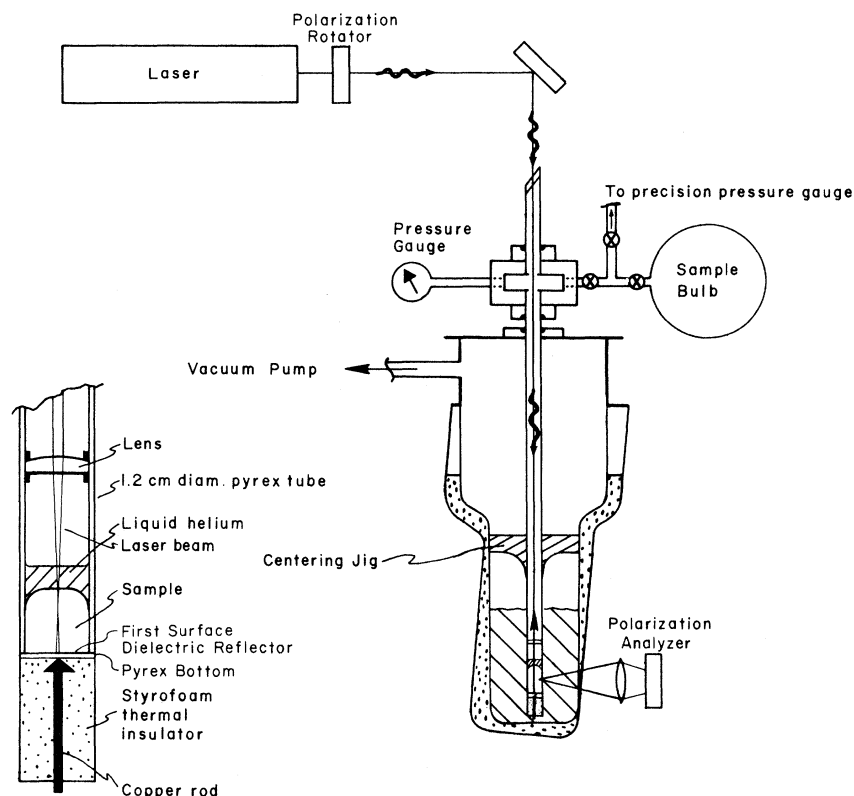


FIG. 2. Simplified diagram of experimental arrangement and details of Raman-scattering cell. The bottom surface of the cell is a dielectric reflector deposited on a Pyrex blank which is cemented to the Pyrex tube with degassed Epoxy cement (Epibond 121 with 9816 hardener). The Raman cell could be raised or lowered through the vacuum seal at the top of the cryostat.

aid of the focused light of a microscope lamp, and then the cell very slowly lowered until solidification initiated at the bottom of the cell. Growth began in the shape of a very small plano-convex lens directly above the pointed copper cold finger that was in contact with the Pyrex cell bottom. The growth propagated up and out to the walls and was allowed to proceed upward at a rate of 1–4 cm/h with the solid-liquid interface becoming flat as it moved away from the bottom (a typical sample height was 1.5 cm, the diameter was ~ 1.0 cm). Throughout its growth, the crystal was observed between a pair of crossed polarizers, one placed on either side of the Dewar tail, that could be conveniently rotated while being maintained in the crossed condition. Due to the birefringence of the uniaxial hcp phase, crystal-grain boundaries were clearly visible. Such boundaries could be detected very early in the growth and if any appeared the crystal was remelted and growth restarted. Any excessive strain was visible through the crossed polarizers as a coloration. At the completion of solidification the upper surface of the sample had the same shape as the liquid meniscus, concave upward. If at this stage the cell was further cooled, cracking in all parts of the sample generally resulted, being particularly severe for para- D_2 . To avoid this problem, which was due to sticking of

the sample to the glass walls and subsequent negative pressure on contraction, the sample was held at a temperature just below the triple point, the temperature being monitored via the vapor pressure. Due to the temperature gradient in the cold helium gas surrounding the cell, the upper sides of the sample were warmer than the center of the top surface of the sample (which was cooled by conduction to the cold finger), and by sublimation and redeposition the sample shape was transformed into the convex form shown in Fig. 2. Very careful cooling, during which the optically monitored strains in the sample were not allowed to become too severe, then resulted in the entire sample pulling away from the vertical walls and the crystals normally remained crack and strain free on further cooling to 4.2 K. The samples used to obtain the present spectra had no apparent grain boundaries or visible cracks and were assumed to be single crystals of the hcp phase. In principle, the c -axis direction could be determined by the optical birefringence, but the possible existence of strain that was predominantly along the tube axis could confuse the results. Instead, the direction of the c axis was determined by the polarization properties of the Raman active optical phonon of the hcp phase.²⁷ For one of the para- D_2 crystals the angle between the c axis and the axis of

the scattering tube (z or vertical direction) was determined to be less than 14° ; the actual angle could be considerably less than this upper bound which was arrived at through consideration of the signal-to-noise ratio of the optical-phonon polarization ratios. For other crystals the bound was not as carefully determined, but for all of the spectra discussed in the present paper, to within experimental error the c axis was always in the vertical direction.

The possibility of the sample temperature being higher than the helium bath surrounding the cell was checked by monitoring the transition temperature via the Raman spectrum. The differential, which could be caused by infrared radiation funneling down the scattering tube or by absorption of laser light, was found to be less than 0.1 K. When knowledge of the temperature was critical, about 0.5 cm of helium was condensed in the Raman tube, on top of the sample, the vapor pressure of which served as a thermometer.

C. Raman spectrometer

Except for a novel frequency-calibration system, the Raman spectrometer was of standard design. The exciting source was the 5145-Å line of a Coherent Radiation Laboratories model 52 argon ion laser operating in the power range 0.1 to 0.7 W. Right-angle scattering was observed using a Spex model 1400 double monochromator and a cooled I.T.T. FW-130 photomultiplier whose output was detected with a Keithley model 301 operational amplifier connected for current detection. In previous experiments^{8,11} the major source of error in determining the frequency shifts of Raman features has been the irregularity and irreproducibility of the spectrometer drive. For the present work a calibrator was devised²⁴ which can achieve accuracies better than 0.05 cm^{-1} . By means of a 180° mirror segment mounted on a 20-Hz chopper wheel, the Raman light and a spectral comb generated with a Fabry-Perot etalon illuminated by white light were fed alternately into the monochromator. The output from the current amplifier was separated into a Raman channel and a calibration channel by two gated amplifiers, and then recorded simultaneously with a two-pen recorder. By calibration with 13 lines of neutral neon, the fringe spacing for the etalon used in these experiments was determined to be 2.0562 cm^{-1} . (In this paper the reciprocal centimeter is used exclusively as an energy or frequency unit, $\bar{\nu} = \nu/c$.) The absolute position of the fringes with respect to the laser line usually held to within 0.01 cm^{-1} over periods of several hours. This implies an extremely stable fringe spacing of

order $\Delta\bar{\nu}/n$ or 10^{-5} cm^{-1} . In most cases the accuracy to which a feature could be located was limited by the irregularity of the spectrometer drive between fringe peaks or by the noise on the fringe pattern. The latter limitation could be easily relieved by using etalon mirrors of lower reflectivity.²⁴

D. Scattering cell

The final configuration of the scattering cell, which underwent a number of design changes in order to optimize the quality of the hydrogen crystals, was extremely simple. Shown in Fig. 2, it consisted of a 1.2-cm-o.d. Pyrex tube with a Brewster window on one end, and bonded to the other end a first surface dielectric reflector positioned accurately perpendicular to the tube axis. Inside the tube was mounted a quartz condensing lens of about 5-cm focal length. The laser beam entered the cell vertically, and when properly aligned was reflected back out of the cell by the dielectric mirror. The advantage of this arrangement was that the laser beam never passed through the Dewar walls and ordinary Pyrex Dewars without optical windows could be used. The quality of the glass was sufficient for adequate imaging of the focussed beam on the spectrometer slits. The polarization properties of the cell were carefully checked: polarized light emitted from the region of focus of the condensing lens was not measurably depolarized, and both polarizations were transmitted with equal amplitude. Noise in the output Raman signal due to bubbles in the liquid helium was undetectable, whereas bubbles in the liquid-nitrogen jacket were excluded from the critical area by the simple expedient of tilting the outer Dewar until it contacted the inner Dewar near the exit beam.

III. RESULTS: LIBRONS

All spectra were obtained using the scattering geometry shown in Fig. 3 where \vec{k}_i and \vec{k}_s denote the incident and scattered light directions, respectively, and XYZ denotes the lab frame. The polarization is indicated by expressions such as XY , YY , etc. where the first and second letters denote the electric field direction of the incident and scattered light, respectively.

Although data have been obtained for several single-crystal paradeuterium and orthohydrogen samples, the bulk of the data to be presented was obtained from a single high-quality paradeuterium crystal grown from gas having an estimated initial concentration of 99% of $J=1$ species. The crystal had the shape of a right-circular cylinder of

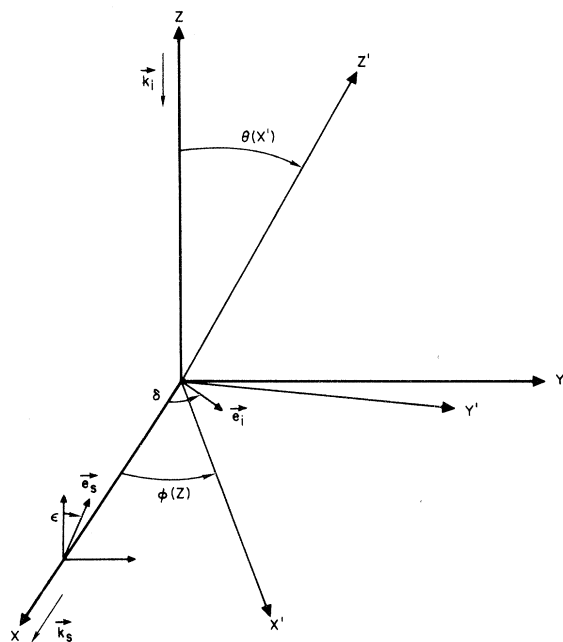


FIG. 3. Scattering geometry used in the experiment. The incident laser beam is along Z and its polarization denoted by δ . The scattered light (polarization given by ϵ) is observed along X .

diameter 1 cm and length 1.5 cm, and all surfaces except the bottom face were free. This ensured that the upper half of the crystal, which was used for the Raman scattering, was well annealed and strain free, and therefore very close to zero pressure. Following the growth, which took approximately $2\frac{1}{2}$ h, spectra of the optical phonon, $J=1 \rightarrow 3$, $J=0 \rightarrow 2$, and $J=1 \rightarrow 1$ reorientational transitions in the hcp phase were recorded at $T=4.2$ K. The polarization properties of the optical phonon were obtained and then the crystal was cooled immediately to 1.16 K. A similar procedure but with faster growth rates ($\frac{1}{2}$ h) was used with ortho-hydrogen samples.

A. Intensities

Spectra taken for frequency shifts $3\text{--}40\text{ cm}^{-1}$ for all four polarizations, XY , XZ , YY , and YZ , in deuterium are shown in Figs. 4 and 5. (There were no other features noted up to about 180 cm^{-1} where the $J=0 \rightarrow 2$ spectrum of ortho- D_2 molecules occurs.) Representative spectra for hydrogen are shown in Fig. 6. No fundamental differences have been noted between the hydrogen and deuterium spectra. Due to the faster conversion rate and generally lower quality of the spectra in hydrogen²⁸ the quantitative analysis has been concentrated on deuterium; in the following sections the dis-

cussion concerns para-deuterium unless otherwise noted. All of these spectra change very little, if at all, when the sample is rotated about an axis coincident with the laser beam. One notes immediately the strong polarization dependence of intensities for the three lower lines which are now identified with the three $\vec{k}=0$ libron modes of the $Pa3$ structure; the shape of the broad upper feature seems to change more than its total intensity, which is consistent with its assignment as a two-libron band. This is in contrast to earlier spectra^{8,11} taken in polycrystalline samples where the spectra were essentially unpolarized. In the present case the cubic ordered phase originates from a single hcp crystal which allows an identification of the symmetry of the modes via the polarization dependence of the intensities.

According to Schuch *et al.*³ the transition from hcp to fcc takes place by a sliding of hexagonal layers relative to one another which requires that the original hcp c direction become one of the $[111]$ directions of the cubic phase. A consideration of the geometry shows that from a single hcp crystal only two cubic crystallites can result, related by a rotation $2\pi/6$ about the original c direction. Further, given a specific fcc arrangement of the molecular centers, there are two ways in which orientational order could lead to the expected $Pa3$ structure. This results in a second type of domain analogous to a magnetic domain. Thus for this structure, the present sample could have up to four types of cubic crystallites, each having a $[111]$ direction along the original c direction which was, to within an uncertainty of 14° , along the vertical or Z direction. Calculations of the $\vec{k}=0$ libron intensities for the $Pa3$ structure (see Appendix A) show that for the present situation the spectra should not change when the crystal is rotated about the Z axis, which is consistent with experiment. A comparison of the experimental and theoretical polarization dependencies is given in Table I. The experimental values were obtained by integration of the experimental traces. In the cases of overlap, the lines were separated by assuming identical profiles for all of the lines. The theoretical intensities (shown in parentheses) were normalized such that for each mode the sum over the four polarizations was equal to the corresponding sum over the experimental intensities. This serves to suppress theoretical information on relative mode intensities, which is model dependent, from the polarization dependencies which are a function only of the crystal symmetry. The agreement is seen to be reasonably good although the experimental polarization dependence of the two T_g modes appears to be systematically weaker than

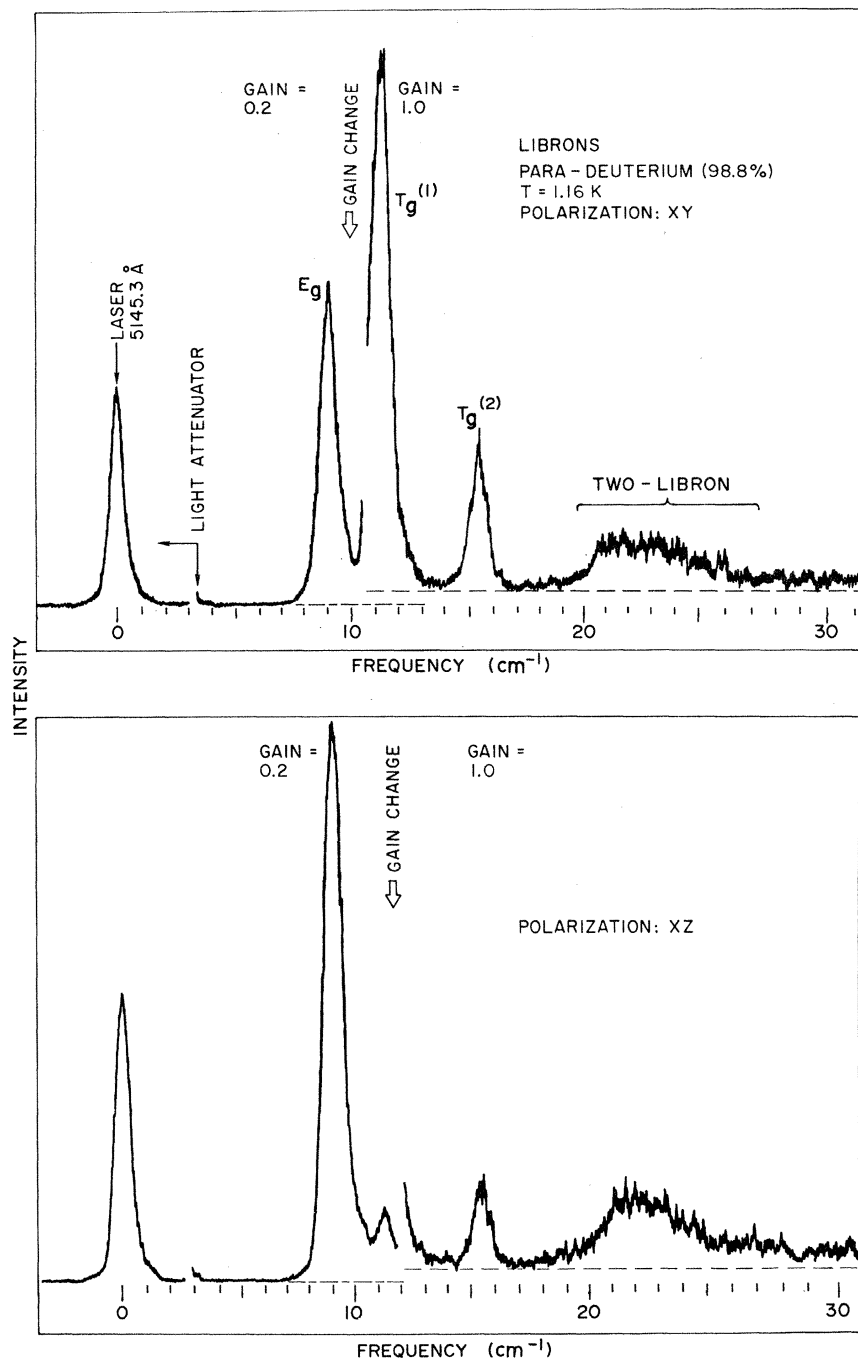


FIG. 4. Libron spectra observed in oriented crystals of 98.8% para- D_2 for polarizations XY and XZ. The monochromator scans from right to left, and as the position of the intense unshifted laser light is approached a piece of Teflon is placed in the exit beam to provide suitable attenuation.

the calculated variation. There is considerable experimental error for the $T_g^{(1)}$ mode because of its overlap with the much stronger E_g mode. The rest of the discrepancy is probably due to a finite deviation of the original c axis from the Z direction. This conjecture was tested by calculating

intensities for orientations deviating slightly from the cubic $[111]$ axis being along the laboratory Z axis. Although an exact fit was not obtained with any of the few orientations tried, it was concluded that a deviation less than 14° could easily reduce the discrepancies to the level of the error.

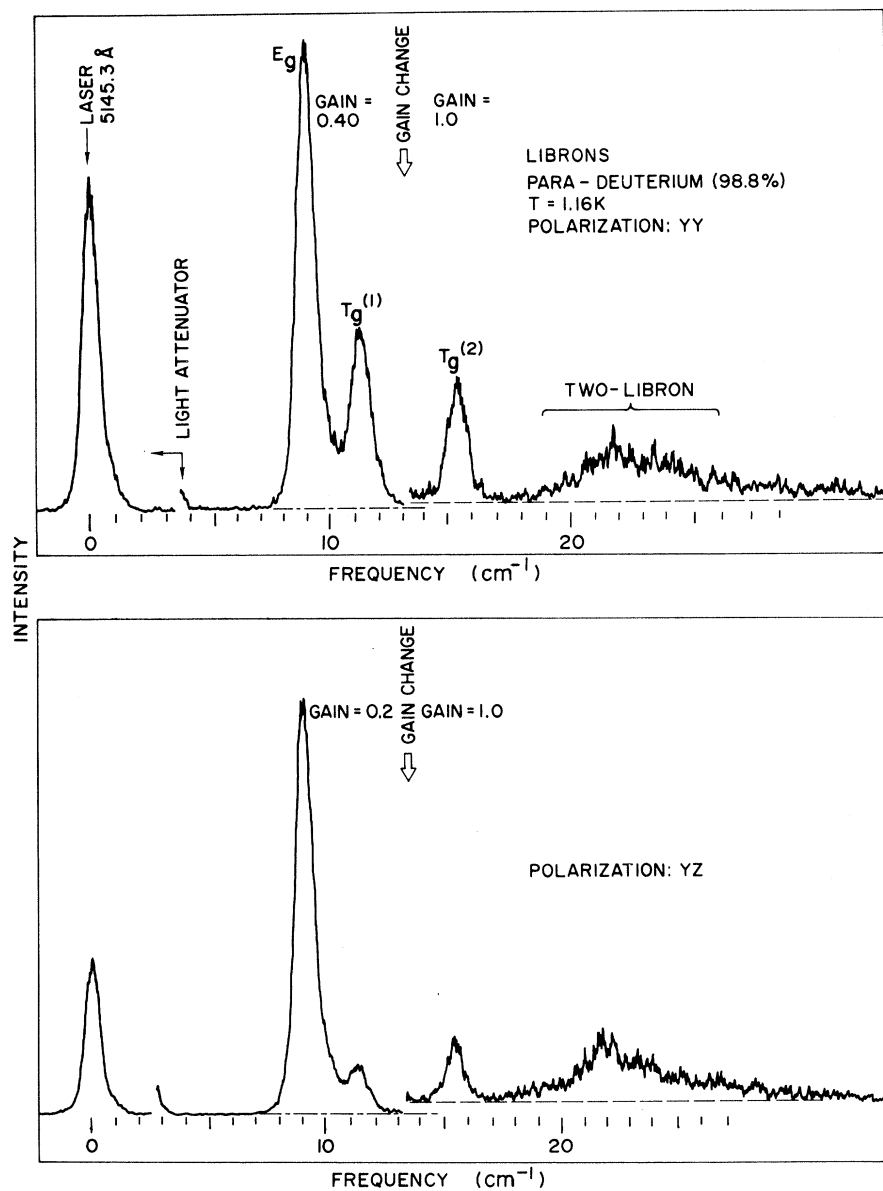


FIG. 5. Libron spectra for same conditions as in Fig. 4, except polarizations are YY and YZ.

B. Frequencies

The libron frequencies, taken to be the frequency shifts at the peaks of the features, were measured as a function of the time that the sample was solid. Because of conversion the $J=1$ concentration continually decreases in time. This change in concentration was determined via the relative intensities of the $J=0 \rightarrow 2$ and $J=1 \rightarrow 3$ transitions.¹¹ This not only enabled a direct determination of the conversion rate, but also enabled a determination of the libron frequencies as a function of concentration. The latter results could be extrapolated to give frequencies for 100% $J=1$ species, as is shown in Fig. 7. For the E_g and $T_g^{(2)}$ modes

the frequencies were fitted by least squares to a straight line $\nu = \nu_0[1 - K(1 - X)]$, where X is the fractional concentration of $J=1$ species. (The $T_g^{(1)}$ mode was not easily separated from the E_g mode at the lower values of X and in order to extrapolate to $X=1$ an average value of K for the E_g and $T_g^{(2)}$ modes was chosen.) The values of K so obtained are listed in Table II. For deuterium, where the accuracy is highest, the values are 1.42 and 0.57 for the E_g and $T_g^{(2)}$ modes, respectively. This is in contrast to molecular-field theories that would predict $K=1$ for the average libron energy, and also differs considerably from the value $K=1.8$ derived from specific heat and $(\partial P/\partial T)_V$ measurements.¹⁹ There is not necessarily any conflict

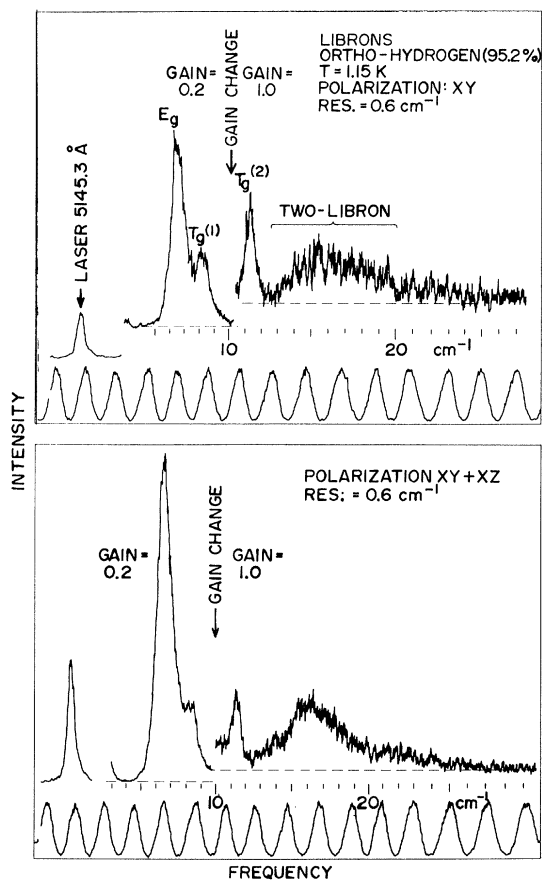


FIG. 6. Libron spectra in 95.2% ortho- H_2 for polarizations XY and $XY+XZ$.

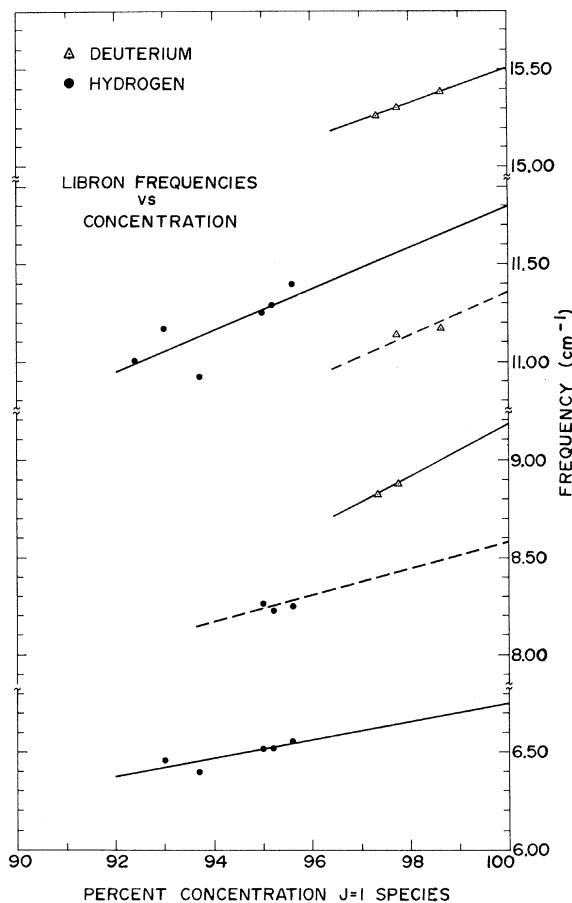


FIG. 7. Low-temperature libron frequencies in p - D_2 and o - H_2 as a function of concentration of the $J=1$ species. The solid lines are least-square fits, whereas the slopes of the dotted lines are averages of the appropriate solid lines (see text).

TABLE I. Comparison of experimental and theoretical libron intensities for para-deuterium.

Mode	Frequency (cm^{-1})	Intensity (Relative)				Intensity for Powder (Relative)		
		XY	XZ	YY	YZ	Expt.	a	b
p - D_2 (98.8%)								
E_g	9.18	0.36 (0.333)	0.67 (0.667)	0.35 (0.333)	0.62 (0.667)	1	1	1
$T_g^{(1)}$	11.35	0.13 (0.114)	0.077 (0.0573)	0.13 (0.172)	0.064 (0.0573)	0.26	0.211	0.318
$T_g^{(2)}$	15.50	0.028 (0.0254)	0.017 (0.0127)	0.030 (0.0383)	0.014 (0.0127)	0.060	0.080	0.042
Two-libron		0.078	0.103	0.095	0.082	0.18 ^c	0.25	...

^a Coll and Harris (Ref. 16), anharmonic self-consistent.

^b Nakamura and Miyagi (Ref. 29), harmonic.

^c Since the detailed polarization dependence of the two-libron feature is not known, the equivalent powder intensity cannot be obtained from the present data in a rigorous way. The quantity given is an average over the four polarizations, appropriately normalized.

TABLE II. Experimental libron frequencies extrapolated to 100% ($J=1$) species and zero temperature. K is the slope of the libron frequencies vs ($J=1$) concentration, and is derived from a least-squares fit to the experimental data (see text). The results are compared to current anharmonic theories with and without virtual ($J=3$) processes.

	K	ν_0 (cm^{-1})	Theory [without ($J=3$) corrections] ^{a,b}	Γ_{eff} [without ($J=3$) corrections] (cm^{-1})	Γ_{eff} [with ($J=3$) corrections] ^b (cm^{-1})
D ₂					
E_g	1.4	9.18 ± 0.05	11.29Γ ± 3%	0.813 ± 0.024	0.740 ± 0.024
$T_g^{(1)}$...	11.35 ± 0.1	14.07Γ ± 4%	0.807 ± 0.033	0.747 ± 0.033
$T_g^{(2)}$	0.6	15.50 ± 0.05	19.55Γ ± 11%	<u>0.793 ± 0.090</u>	<u>0.749 ± 0.090</u>
			Weighted average	0.810 ± 0.019	0.743 ± 0.019
H ₂					
E_g	0.7	6.75 ± 0.15	11.29Γ ± 3%	0.598 ± 0.022	0.575 ± 0.022
$T_g^{(1)}$...	8.58 ± 0.2	14.07Γ ± 4%	0.610 ± 0.027	0.591 ± 0.027
$T_g^{(2)}$	0.9	11.80 ± 0.2	19.55Γ ± 11%	<u>0.604 ± 0.066</u>	<u>0.590 ± 0.066</u>
			Weighted average	0.603 ± 0.017	0.582 ± 0.017

^aSee Ref. 16.

^bSee Ref. 19.

between the latter result and the present values of K : Raman measurements determine the concentration dependence of the $\vec{k} \approx 0$ librions only, whereas thermodynamic quantities are determined by the libron density of states involving all values of \vec{k} . As yet there is no detailed theory for libron frequencies as a function of $J=0$ impurities.

The experimental libron frequencies extrapolated to $X=1$ are given in Table II along with the most recent theoretical results of Coll and Harris¹⁶ for the $\vec{k}=0$ librions. In order to display the very good agreement between theory and experiment for the libron-frequency ratios, a value of Γ_{eff} was determined for each mode. A maximum likelihood value of Γ_{eff} was determined making the crude assumption of independent Gaussian distributions for both experimental and theoretical errors. However, the main uncertainty in Γ_{eff} derives from uncertainties in the theoretical values.¹⁶ Estimates of the latter uncertainties¹⁶ are only approximate and therefore the over-all error given for Γ_{eff} is not very meaningful. The excellent fit for the frequency ratios would seem to indicate that these errors have been overestimated.

Recently, Harris *et al.*¹⁹ have further refined the theory of the libron frequencies by including the effect of virtual $J=3$ processes. In the approximation of a common shift for all $\vec{k}=0$ libron modes, they found the libron energies to increase by

$$\Delta E_0 = 45.21\Gamma^2/B,$$

which amounts to about a 10% shift for D₂ and 3.5% shift for H₂. The last column in Table II gives the values of Γ_{eff} when the $J=3$ corrections are included. One notes some improvement in the variation of Γ_{eff} for the different modes. Since the accuracy of the theoretical correction has not been estimated, we have calculated the maximum likelihood value of Γ_{eff} using the errors from the adjacent column in Table II.

Nakamura *et al.*³⁰ were the first to consider the perturbation of $J=3$ states on libron frequencies. They determined the shift for each of the $k=0$ libron modes and obtained $-53\Gamma^2/B$, $-20\Gamma^2/B$, and $-61\Gamma^2/B$ for the E_g , $T_g^{(1)}$, and $T_g^{(2)}$ modes, respectively. These are of the same order as the average shifts calculated by Harris *et al.*¹⁹ but of opposite sign. Very recently, Fujio and Nakamura³⁰ have added the shifts due to polarization of the ground state by an admixture of the ($J=3$, $m_j=0$) state (an effect included in the work of Harris *et al.*¹⁹). The net shifts are now $28\Gamma^2/B$, $46\Gamma^2/B$, and $-13\Gamma^2/B$ for the E_g , $T_g^{(1)}$, and $T_g^{(2)}$ modes, respectively. This gives values of Γ_{eff} for the respective modes of 0.765, 0.746, and 0.807 cm^{-1} for D₂, and 0.584, 0.591, and 0.607 cm^{-1} for H₂. Here the variation in Γ_{eff} is rather large. (See Note added in proof.)

C. Two-libron spectrum

Figure 8 shows the two-libron obtained with the polarization analyzer removed in order to increase the signal-to-noise ratio. Its composite nature is more evident than in previous spectra.^{8, 11, 18} The vertical bars drawn under the spectrum indicate positions and relative intensities of the discrete two-libron excitations calculated by Berlinsky and Harris¹⁷ using a localized model. Here the value 0.802 cm^{-1} used for Γ_{eff} was derived from an earlier analysis of the single-libron spectrum, $X=98.8\%$. The main features of the spectrum are seen to be reproduced fairly well.

Berlinsky³¹ later calculated the complete two-libron spectrum without the simplification of localized excitations and the result is shown as the dashed line in Fig. 8. The librons were treated anharmonically and libron-libron interactions included explicitly. The theoretical spectrum shown has been convoluted³¹ with a Lorentzian function of width 1.25 cm^{-1} in order to approximate the effect of the instrumental resolution. Correspondence between theory and experiment is quite good as far as the general shape is concerned and only a slight adjustment of Γ_{eff} would be required to make the main peaks coincide. Some of the differences may be due to the fact that the theoretical profile is for a powder, not an "oriented" crystal. In addition, the theory considered only nearest-neighbor interactions. An interesting result of the inclusion of libron-libron interactions is that a weak bound state is predicted. In principle this produces a δ function in the spectrum, but after the effect of instrumental broadening

is included it appears only as a small bump to the left of the main peak (indicated by the arrow in Fig. 8). There *may*, in fact, be a corresponding feature in the experimental spectrum, but the signal-to-noise ratio is too low to make a positive assignment.

D. Temperature dependence of libron modes

The temperature dependence of libron modes was studied in a single crystal of 97.6% *p*-D₂. The sample was thermally cycled through the transition five times in order to stabilize the fcc phase.³² Care was taken not to exceed the transition temperature by more than 0.4 K, since at temperatures of order 12 K or higher, the original hcp structure is quickly recovered. The purpose of so preparing the sample was to isolate from the temperature dependence of the librons the complications arising from the fcc to hcp structural change that accompanies the orientational transformation of uncycled samples. Spectra were observed first at the lowest temperatures ($\sim 1.10 \text{ K}$) and then at monotonically increasing temperatures, which were held constant while measurements were made. Representative spectra that were taken are shown in Fig. 9. At 1.10 K the one-libron lines are seen to be sharp, with a width slightly greater than that determined by the instrumental resolution. As the temperature is raised the lines broaden into each other with only minor observable shifts of the scattering maxima toward the lower frequencies. The libron structure remains distinct to within a few centidegrees of the transition temperature T_c , estimated to be

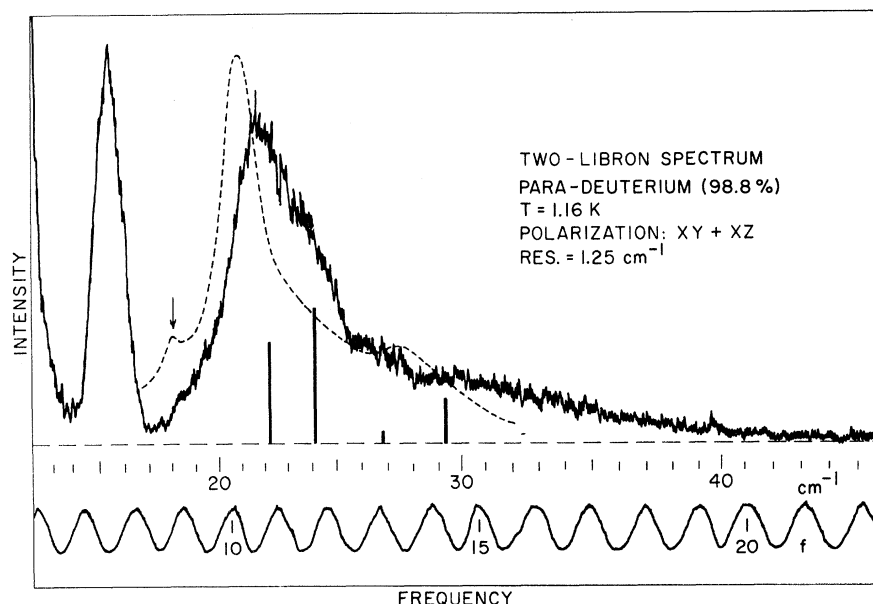


FIG. 8. Two-libron spectrum observed in high-purity (98.8%) para-D₂ at low temperature ($T=1.16 \text{ K}$). The bars are the theoretical results of Berlinsky and Harris (Ref. 17) in the approximation of localized excitations. The dotted curve is the complete two-libron spectrum calculated by Berlinsky (Ref. 31) convoluted with a Lorentzian instrumental line-shape function of width 1.25 cm^{-1} . The arrow indicates a localized mode (δ -function) broadened by the line-shape function.

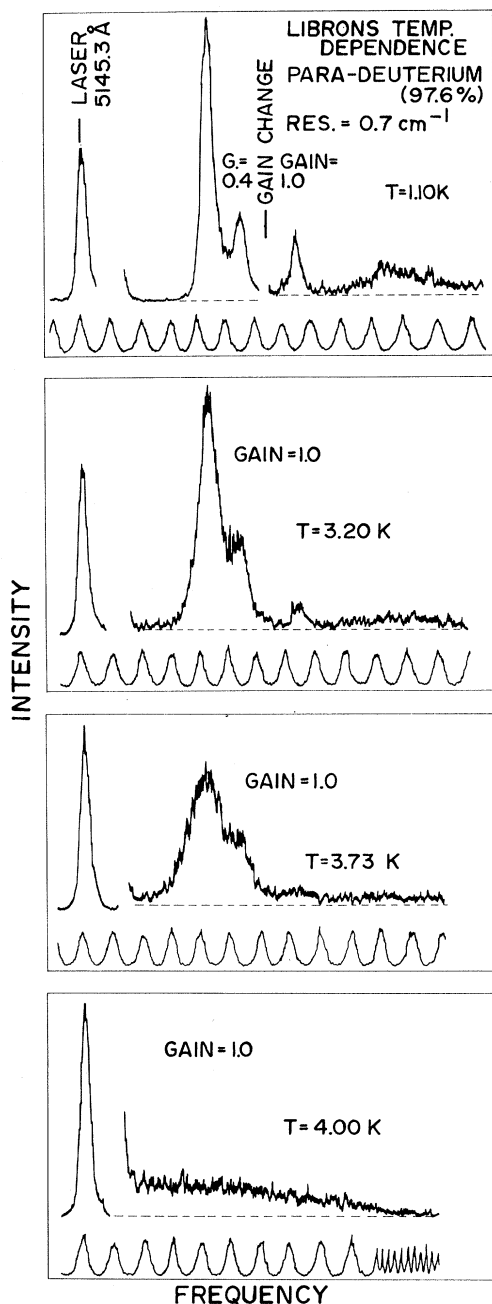


FIG. 9. Traces of libron spectra at several temperatures in 97.6% para-deuterium. The gain may be slightly different for each of the temperatures.

3.854 K from these data and from knowledge of the para-ortho concentration. Above the transition temperature the libron lines disappear completely and are replaced by a very broad scattering spectrum associated with molecular reorientations in the disordered state.³³ These excitations might be called "paralibrons" in analogy with the term paramagnons used for the remnants of mag-

nons above T_c in magnetic materials. It is interesting to note the apparent rapid decrease in intensity of the two-libron band and the $T_g^{(2)}$ mode as the temperature increases.

1. Frequencies

The dependence of the libron frequencies on temperature is shown in Fig. 10 and in reduced form in Fig. 11. The most complete data was obtained for the strong E_g mode. The $T_g^{(1)}$ and $T_g^{(2)}$ modes could only be followed to $0.8T_c - 0.9T_c$ because of line broadening and signal-to-noise problems. The uncertainty in T_c and the breadth of the line precluded reliable data on the E_g mode closer than a few centidegrees of the transition. Up to this region the frequency is seen to have decreased by approximately 4% of the low-temperature value. Such weak temperature dependence is characteristic of first-order phase tran-

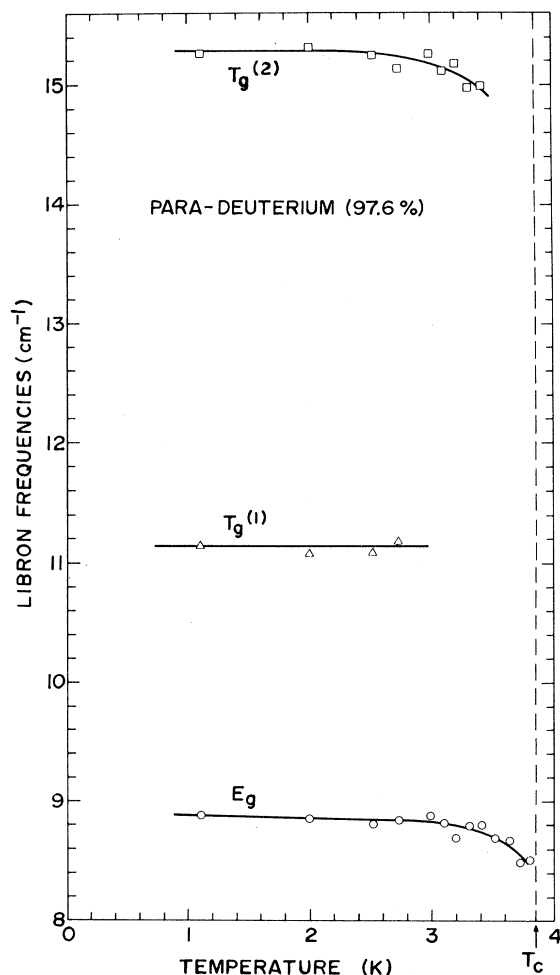


FIG. 10. Temperature dependence of the libron frequencies in 97.6% para-deuterium. The frequencies were taken at the peaks of the respective features.

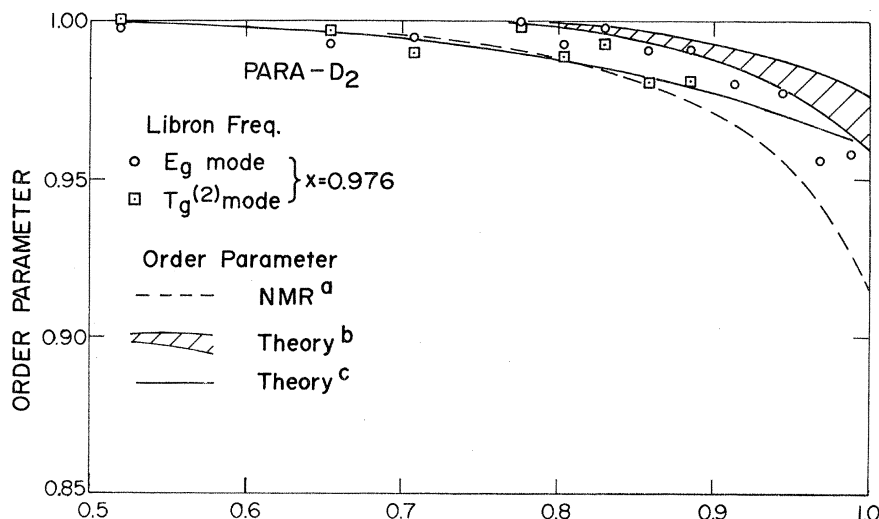


FIG. 11. Order parameter vs T/T_c in para-deuterium as determined by various methods. Open circles and squares: $\bar{\nu}(T)/\bar{\nu}(0)$ for the E_g and $T_g(2)$ libron modes observed in the present experiment ($X=0.976$); the dashed line (a) is the normalized Pake splitting of the NMR absorption line for $J=1$ molecules and is representative of the results of Meyer *et al.* (Ref. 21) for X extrapolated to 1.00, and Hardy and Berlinsky (Ref. 36) for $X=0.98$; the shaded region (b) gives the cluster variation results of Lee and Raich (Ref. 35) for $\langle 1 - \frac{3}{2}J_z^2 \rangle_T$; the upper and lower lines correspond to $T_c = 0.715T_b$ and $0.75T_b$, respectively, where $T_b = 19\Gamma/3k$; the solid line (c) is the corresponding result of Hardy and Berlinsky (Ref. 36) calculated from the libron density of states.

sitions. Although there are no published theories for the temperature dependence of the libron frequencies, it has been pointed out by Raich³⁴ that on the basis of a random-phase approximation (RPA) treatment, one would expect the libron frequencies to be proportional to the orientational order parameter $\langle 1 - \frac{3}{2}J_z^2 \rangle_T$. Lee and Raich³⁵ have calculated the temperature dependence of $\bar{n} = \frac{1}{2}\langle J_z^2 \rangle$ by a cluster-variation method and in Fig. 11 their result for $1 - 3\bar{n} \equiv \langle 1 - \frac{3}{2}J_z^2 \rangle_T$ is plotted vs T/T_c [shaded region (b)]. The range of theoretical values is due to the fact that near the transition there are several structures having very nearly the same free energy and it is difficult to assign a transition temperature. Raich³⁴ suggests that T_c upon warming will occur for values of T/T_b somewhere between 0.715 and 0.75 ($T_b = 19\Gamma/3k$). This predicts values of T_c between 5.24 and 5.5 K, respectively, if the experimental value from the present Raman results $\Gamma_{\text{eff}} = 0.810 \text{ cm}^{-1}$ is used. For purposes of comparing temperature dependencies, the value of T_c was adjusted to equal the experimental value. In view of the experimental error and the approximations made in the theory, the agreement with the reduced libron frequencies is reasonable. Best agreement is obtained with the lower limit of the theoretical range corresponding to larger

T/T_b . Also shown in Fig. 11 are the results of Hardy and Berlinsky³⁶ for

$$\langle 1 - \frac{3}{2}J_z^2 \rangle_T / \langle 1 - \frac{3}{2}J_z^2 \rangle_0,$$

where zero-point libron motion is taken into account and where the temperature-dependent libron occupation number $n(T)$ is determined self-consistently from the theoretical anharmonic density of states.

As a comparison with other experiments, the NMR results of Meyer, Weinhaus, and Maraviglia²¹ and Hardy and Berlinsky³⁶ for the normalized Pake doublet width of the $J=1$ molecules in ordered para-deuterium are also shown in Fig. 11. This quantity should be directly proportional to $\langle 1 - \frac{3}{2}J_z^2 \rangle_T$. The former results were obtained for $J=1$ concentrations X between 0.55 and 0.96 and extrapolated to $X=1.00$; the latter were taken at a fixed concentration $X=0.98$ and are uncorrected. The two sets of NMR data agree quite well and are represented by a single curve but fall somewhat below the Raman data and theory.

We have found no evidence for structural changes to any of the intermediate ordered states that have been the subject of theoretical conjecture.¹² However, a careful search was made only on one 97% para-D₂ sample which had been first thermally cycled.

2. Linewidths

Signal-to-noise considerations limited the study of linewidths to the E_g mode whose lower-frequency side was essentially unperturbed by overlap with other lines. The instrumental broadening, which was important only at low temperatures, was removed according to

$$\Delta\bar{\nu} = [(\Delta\bar{\nu}_{\text{obs}})^2 - (\Delta\bar{\nu}_{\text{inst}})^2]^{1/2},$$

where $\Delta\bar{\nu}_{\text{inst}}$ was determined from the profile of the laser line ($\Delta\bar{\nu}_{\text{inst}} = 0.70 \text{ cm}^{-1}$ for the traces of Fig. 9). The temperature-dependent part of the broadening was then extracted according to

$$B(T) = \{[\Delta\bar{\nu}(T)]^2 - [\Delta\bar{\nu}(T = 1.1 \text{ K})]^2\}^{1/2},$$

where the $\Delta\bar{\nu}$'s and $B(T)$'s are full widths at half-height and $\Delta\bar{\nu}(T = 1.1 \text{ K}) = 0.72 \text{ cm}^{-1}$ for the 96.6% p -D₂ sample. Of course this procedure is rather crude in that the instrumental, static broadening and temperature broadening profiles are not independent Gaussian distributions, and therefore subtracting the squares of their widths does not separate them in general. A deconvolution was not attempted due to the low signal-to-noise ratio. However, because the temperature-dependent part quickly becomes dominant, the shape of the $B(T)$ vs $1/T$ plot, Fig. 12, is not likely to be much affected. As can be seen from Fig. 12, the broadening process is reasonably well described by an activation energy, of magnitude 15.3 K or 10.7 cm^{-1} . This falls quite close to the central peak of the one-libron density of states calculated by Berlinsky and Coll³⁷ in a self-consistent anharmonic approximation. This point will be further

commented on in the discussion.

E. Line shapes

One might expect that the temperature-dependent part of the broadening would have a Lorentzian profile, characteristic of lifetime broadening. However, a detailed examination of the low-frequency side of the E_g mode showed this not to be the case. In Figs. 13(a) and (b) are presented the smoothed experimental data for temperature 3.414 and 3.73 K, respectively ($T_c = 3.854 \text{ K}$). The error bars indicate limits on the data for maximum possible shifts in the baseline from which the signal amplitude is measured. In one case, Fig. 13(b), the baseline cannot be shifted downward and the bars allow for possible scattered light from a broadened line centered at zero-frequency shift. There are additional errors not shown, namely, statistical errors in the amplitude due to noise, and small irregularities in the frequency scale due to nonuniform grating drive; these do not affect the basic features.

For both temperatures the line shape seemed to be intermediate between a Lorentzian and a Gaussian. This prompted a fitting of the shape with their convolution

$$I(\bar{\nu}) = \int_{-\infty}^{+\infty} \{e^{-t^2} / [y^2 + (t - \bar{\nu})^2]\} dt,$$

where y controls the relative widths of the separate distributions.³⁸ The solid lines in Figs. 13(a) and (b) are for $y = 0.5$, which is equivalent to a ratio 1.67 for the Gaussian to Lorentzian width. In both cases the fit is remarkably good and certainly

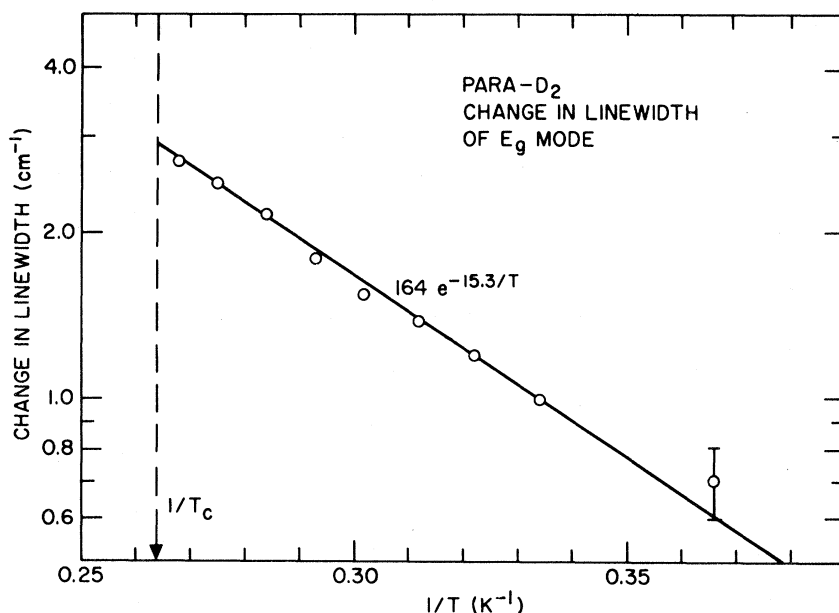


FIG. 12. Change in linewidth (full width at half-height) of E_g mode in 97.6% p -D₂ as a function of $1/T$. The instrumental linewidth and temperature-independent part of the linewidth have been removed (see text). The straight line is given by $164 e^{-15.3/T}$.

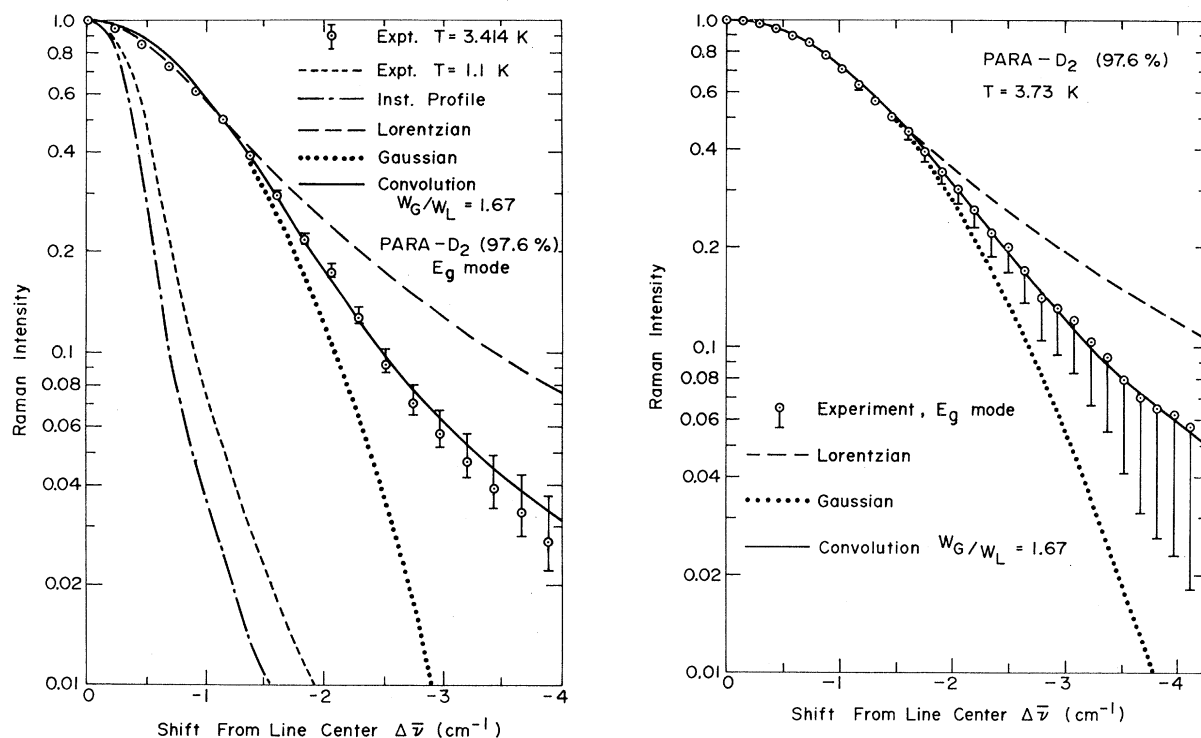


FIG. 13. Observed low-frequency Raman-intensity profile of the E_g mode in 97.6% para-deuterium for (a) $T=3.414$ K and (b) $T=3.73$ K. Also shown are the spectrometer profile, the profile of the E_g mode at $T=1.1$ K, and several theoretical lineshapes. The solid curves are proportional to the convolution of a Gaussian and a Lorentzian shape, where in both figures the ratio of the respective widths W_G/W_L has the value 1.67.

partly fortuitous since the instrumental and impurity broadening has not been removed. However, the behavior of the tail of the profile, where these disturbances are negligible, allows one to draw the conclusion that for 97.6% $J=1$ p - D_2 the temperature-induced broadening is not a simple lifetime effect.

IV. RESULTS: $\Delta J=2$

A. $J=0 \rightarrow 2$ impurity spectrum

The pure rotational Raman spectrum due to the $\sim 1.2\%$ orthodeuterium molecules in an oriented crystal of para-deuterium consists of four features and is shown in Figs. 14 and 15. Except for different relative intensities of the features the spectrum is essentially identical to that obtained previously in a polycrystalline specimen.¹¹ The frequencies, which agree remarkably well with the earlier less accurate values, are given in Table III. For hydrogen, the values in the table were obtained by extrapolation to 100% $J=1$ species from a study of their concentration dependence. (See Fig. 16. Also included are the corresponding results of Prior³⁹ and the infrared-absorption results of Clouter *et al.*⁴⁰ for 99% ortho- H_2 .) The

frequencies are also expressed relative to an estimated origin $\bar{\nu}_0$ of the $J=0 \rightarrow 2$ transitions (the single frequency that would be observed if the anisotropic intermolecular interactions were switched off). Since, as will be seen, there is presently no satisfactory theory for the splittings, the origin cannot be deduced from the impurity spectrum itself. Instead, the theory of Van Kranendonk⁴¹ for the $J=0 \rightarrow 2$ roton triplet in pure $J=0$ samples was used to extract $\bar{\nu}_0$ from the data of McTague *et al.*⁴² According to Van Kranendonk,⁴¹ $\bar{\nu}_0 = \bar{\nu}_2 - \frac{1}{5}\Delta$, where $\bar{\nu}_2$ is the frequency of the center component of the triplet and Δ the spacing of the lines, which leads to a value $\bar{\nu}_0 = 178.66$ cm^{-1} . Although derived for the hcp form of the solid at a slightly different density from the fcc phase, this value should be quite reliable since the total change in $\bar{\nu}_0$ in going from gas to solid is only 0.9 cm^{-1} .⁴³

The $J=0 \rightarrow 2$ spectrum in the fcc phase is of particular interest in that the spectrum of essentially isolated $J=0$ molecules should reflect the molecular site symmetry in a straightforward manner. In the $Pa3$ structure the molecular site symmetry is C_{3i} , which requires the $J=2$ state to split into three components, $m_J = 0, \pm 1, \pm 2$, where m_J is

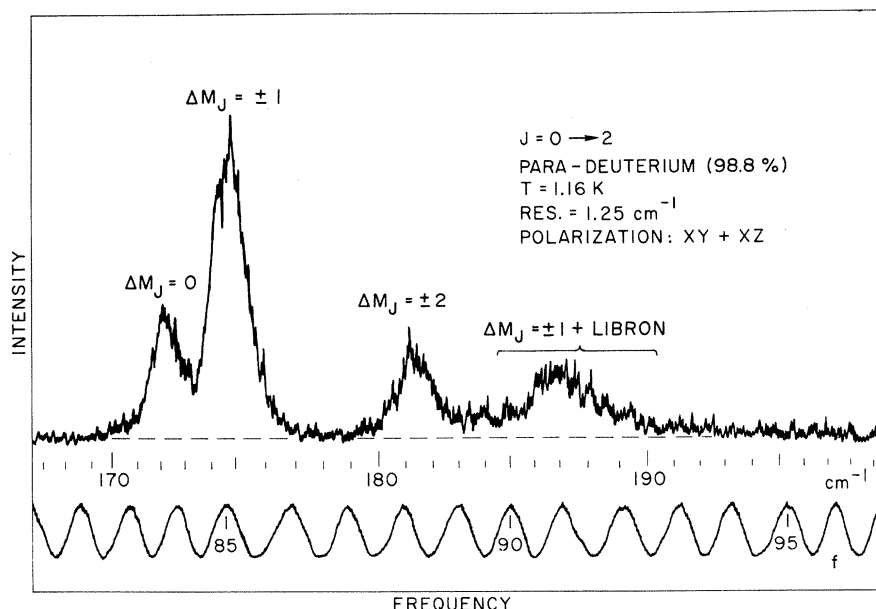


FIG. 14. $J=0 \rightarrow 2$ Raman spectrum of impurity ortho- D_2 molecules in ordered solid para- D_2 ($X=0.988$), along with proposed assignments. The transitions are from the $|0,0\rangle$ to the $|2,M_J\rangle$ states and are conveniently labeled by the change in M_J . The broad feature at higher frequencies is thought to be due to a transition in the impurity molecule with $\Delta J=2$, $\Delta M_J=\pm 2$, accompanied by the creation of a libron in the host $J=1$ molecules.

the projection of J along the axis of symmetry. If one assumes that neighboring $J=1$ molecules are not perturbed by the presence of a $J=0$ impurity, the frequencies can be calculated in the molecular-field approximation using the result of Raich and James⁴⁴ for the effective potential (summing over nearest neighbors):

$$V_{\text{eff}} = - (95\Gamma_0/6)(3 \cos^2\gamma - 1), \quad (1)$$

where γ is the angle between the internuclear axis and the symmetry axis. For a molecule in the $J=2$ state one obtains for the energies

$$\epsilon_0 = -2d, \quad \epsilon_{\pm 1} = -d, \quad \epsilon_{\pm 2} = 2d, \quad (2)$$

where $d = 95\Gamma_0/21$.

If the sum is taken over all neighbors the energies in Eqs. (1) and (2) are increased by the factor 1.118. The results, replacing Γ_0 with $\Gamma_{\text{eff}} = 0.81$, are shown in Fig. 17 along with experiment. Also included for completeness are results calculated for two of the orientational orderings studied by James.¹² There is no agreement, even qualitative, with any of the patterns. This lack of agreement prompted the conjecture that the spectrum consists of the three expected $J=0 \rightarrow 2$ transitions corresponding to the $Pa3$ site symmetry plus a libron combination band at higher frequencies, with a resulting depression in frequency of the $\Delta m_J = \pm 2$ transition in analogy to the effect of the two-libron band on the single-libron frequencies.

The present $J=0 \rightarrow 2$ spectra were obtained in single crystals and hence in principle the lines should be identifiable by their polarization properties. Table IV compares intensities calculated for

the $Pa3$ structure assuming the molecule sits in a potential of the form given by Eq. (1), along with the experimental intensities derived from the data shown in Fig. 15.

Except for the $\Delta m_J = 0$ transition, the theoretical polarization dependencies which have to be averaged over the various crystal-field axes present in our "oriented crystal," are rather weak. This, coupled with the rather low accuracy of the experimental intensities, precludes a positive identification of any but the $\Delta m_J = 0$ transition, although the general trends appear to be consistent with the high-frequency feature being the combination band.

In a less rigorous way one can complete the assignment by noting that the three lowest features have linewidths considerably narrower than the upper feature: Separating out the instrumental broadening as before, the lowest lines are seen to have very nearly the same width, 0.6 cm^{-1} , whereas the upper feature has a half-width of at least 2.5 cm^{-1} which suggests that it should be associated with the libron combination band. Furthermore, the peak of the upper feature is displaced from the $\Delta m_J = \pm 1$ line by an amount corresponding almost exactly to the main peak of the anharmonic single-libron density of states calculated by Berlinsky and Coll.³⁷ One can distinguish very weak structure near 184 cm^{-1} , the region appropriate to librons in combination with the $\Delta m_J = 0$ transition. One could argue that the weakness (or absence) of such a band is due to the fact that the $|J, m_J\rangle = |2, 0\rangle$ state is rather similar to the $|1, 0\rangle$ ground state of the para neighbors and therefore couples weakly to the librons. Carrying this picture further one would expect the

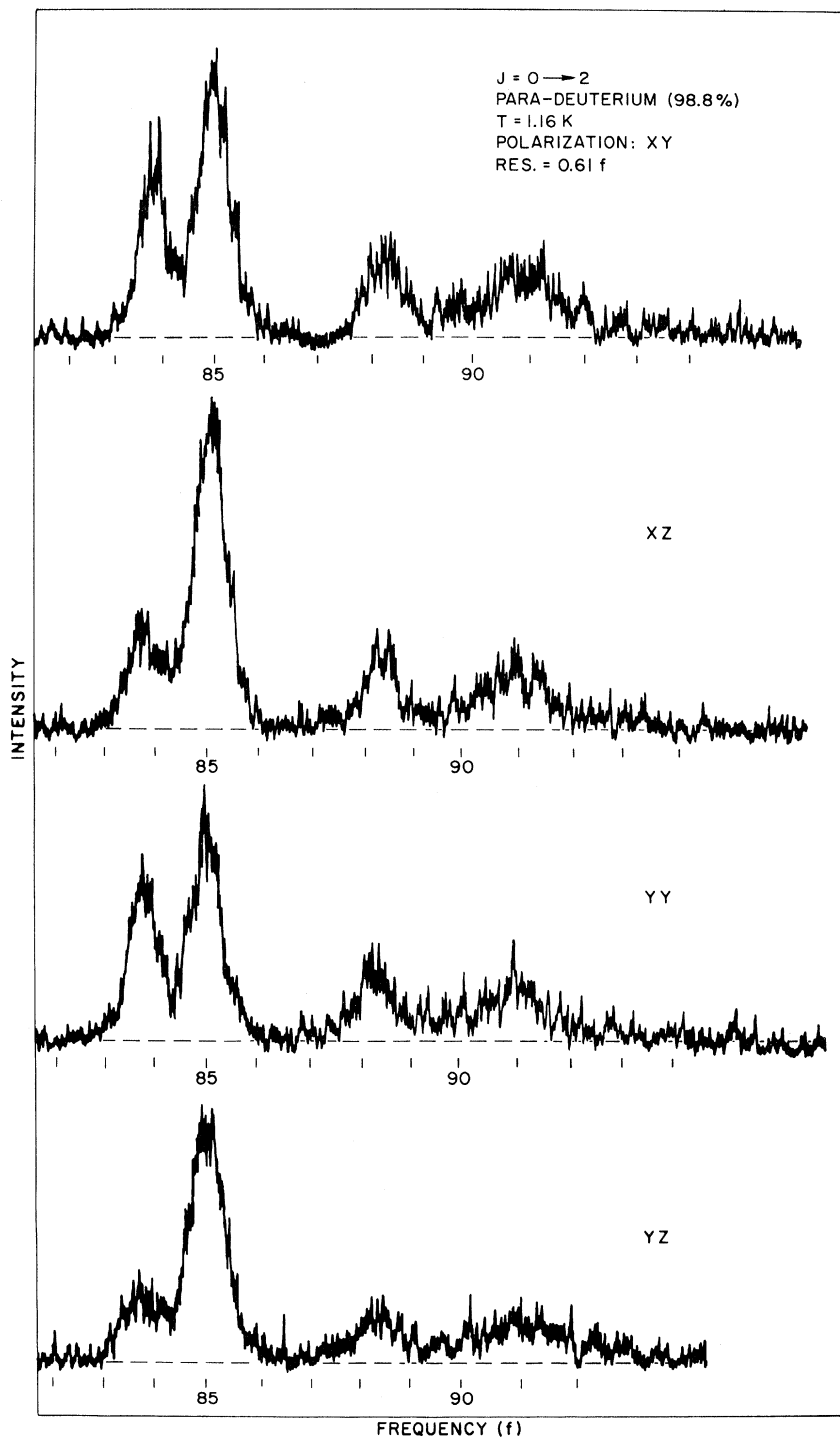


FIG. 15. Polarization dependence of the $J=0 \rightarrow 2$ spectrum of impurity ortho- D_2 molecules in ordered para- D_2 ($X=0.988$).

$|2, \pm 2\rangle$ states, which most resemble the $|1, \pm 1\rangle$ single-molecule excited states, to be very strongly coupled to the librins. This is in accord with the large shift and anomalous intensity of the $\Delta m_J = \pm 2$ line. The corresponding combination band, however, seems to be either missing or

extremely weak.

Boggs *et al.*⁴⁵ have independently given analogous assignments to the $J=0 \rightarrow 2$ sidebands observed in the infrared fundamental band of 99.7% *orthohydrogen*. The signal-to-noise ratio was quite high and a fairly convincing fit to the upper feature was

TABLE III. Frequencies of $J=0 \rightarrow 2$ transitions in fcc p -D₂ and o -H₂.

Proposed assignment	D ₂ (98.8% $J=1$; $T=1.16$ K)		H ₂ (100% $J=1$ ^a ; $T=1.15$ K)	
	$\bar{\nu}$ (cm ⁻¹)	$\Delta\bar{\nu}$ (cm ⁻¹)	$\bar{\nu}$ (cm ⁻¹)	$\Delta\bar{\nu}$ (cm ⁻¹)
$\Delta m_J = 0$	172.15 ± 0.1	-6.51	347.92 ± 0.38 (347.91) ^b	-5.47
± 1	174.75 ± 0.1	-3.91	350.36 ± 0.38 (350.17) ^c	-3.03
± 2	181.33 ± 0.15	2.67	354.43 ± 0.9 (355.07) ^b	1.04
Combination	186.78 ± 0.2	8.12	359.35 ± 1.2 (359.27) ^b	5.96
		$\bar{\nu}_0 = 178.66$ ^c		$\bar{\nu}_0 = 353.39$ ^c

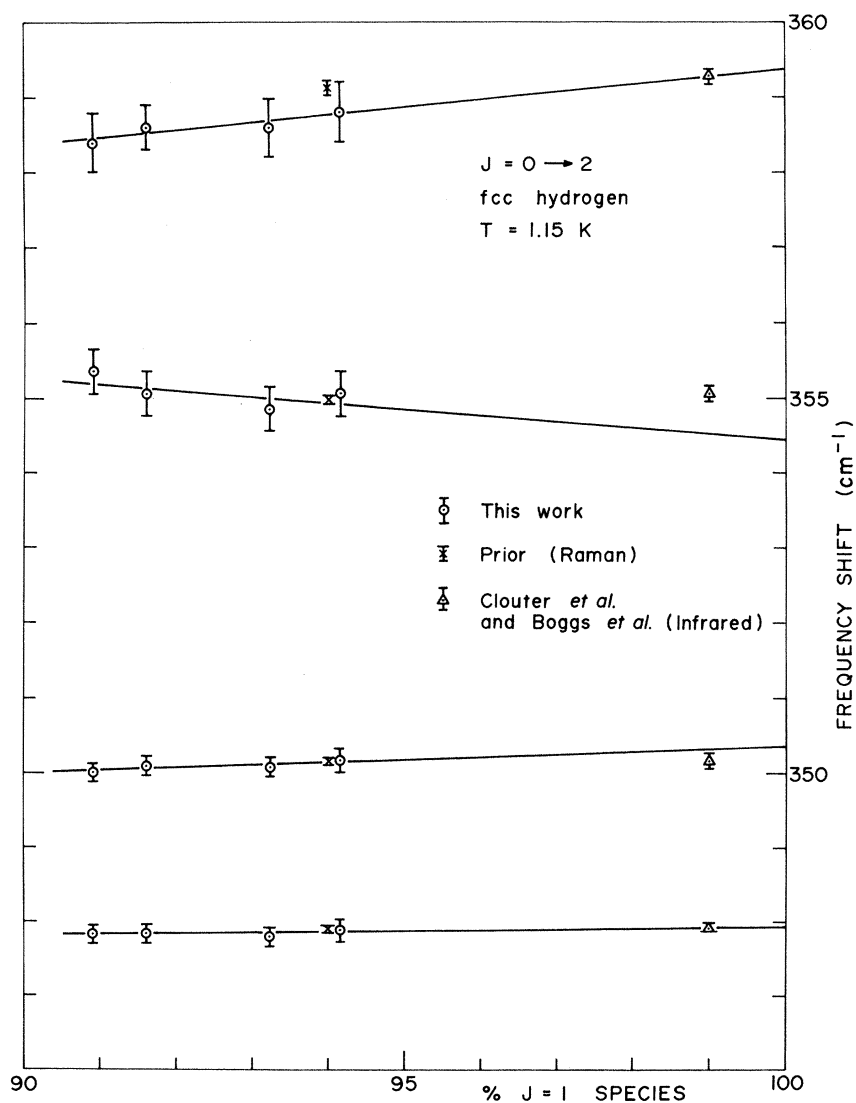
^aExtrapolated.^bFrom infrared-absorption results of Clouter, Gush, and Welsh (Ref. 39) for 99% orthohydrogen.^c $\bar{\nu}_0$ is derived from the $J=0 \rightarrow 2$ roton triplet in nearly pure $J=0$ samples; see text.

FIG. 16. Frequencies of the $J=0 \rightarrow 2$ features in ordered orthohydrogen as a function of $J=1$ concentration. The straight lines are least-squares fits to the present Raman data. Included for comparison are the corresponding results of Prior (Ref. 39), and frequencies from the near-infrared absorption spectra of Clouter *et al.* (Ref. 40) and Boggs *et al.* (Ref. 45) (the $J=0 \rightarrow 2$ features are observed in combination with a vibron transition in the $J=1$ host).

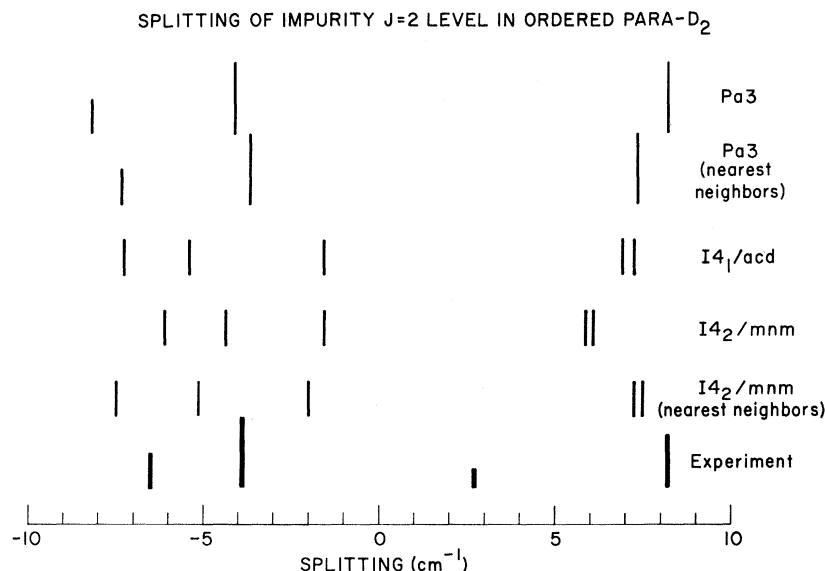


FIG. 17. Comparison of experimentally observed splittings of the $J=2$ state of ortho- D_2 in ordered para- D_2 with simple molecular-field predictions for various structures. The theoretical model ignores tipping corrections, i.e., the orientations of the $J=1$ host molecules are assumed to be unaffected by the presence of the $J=0$ impurity.

made by convoluting the $\Delta m_J = \pm 1$ profile with an approximation to their results for the libron band (observed as a combination with a vibron). The same procedure applied to the $\Delta m_J = 0$ transition yielded a peak that also corresponded well to the experimental spectrum. This feature is very sensitive to impurity concentration and has been observed only in a very pure sample (99.7%).

For completeness the $J=0 \rightarrow 2$ impurity spectra for para- D_2 and ortho- H_2 in the disordered phase

are presented in Fig. 18. The marked asymmetry is very likely due to the considerable short-range order of the $J=1$ molecules that exists close to the transition temperature. The high-energy wing of the line derives from the creation of a $J=0 \rightarrow 2$ roton plus a "para-libron." The lack of thermal excitation of the high-frequency "para-librons" explains the absence of the low-energy wing, since it derives from the creation of a $J=0 \rightarrow 2$ roton plus the *destruction* of a "para-libron."

TABLE IV. Theoretical intensities of $J=0 \rightarrow 2$ transitions of $J=0$ impurities for an "oriented" crystal in the ordered fcc phase. Experimental values for 98.8% para- D_2 at 1.16 K are given in parentheses. Here, $\Delta = (\frac{2}{15} \pi)^{1/2} (\alpha_{\parallel} - \alpha_{\perp})$.

Polarization	Multiplier	$\Delta m_J = 0$	Transition intensity		Combination
			$\Delta m_J = \pm 1$	$\Delta m_J = \pm 2$	
Powder average					
XZ		2	4	4	
XY	$\frac{1}{5} (\Delta^2/4\pi)$	2	4	4	
YZ		2	4	4	
YY		$\frac{8}{3}$	$\frac{16}{3}$	$\frac{16}{3}$	
[111] axis along Z axis ^a					
XZ		6(7.3)	28(23.3)	20(5.3)	(4.3)
XY	$\frac{1}{27} (\Delta^2/4\pi)$	12(13.2)	20(20.1)	22(6.1)	(4.9)
YZ		6(6.3)	28(21.7)	20(4.7)	(4.1)
YY		18(15.2)	24(19.9)	30(6.3)	(4.9)
XY+XZ		18(18)	48(42)	42(15)	(21)

^a The values in parentheses are those experimentally determined from the peak heights of the features and are normalized such that the sum over the four polarizations for the $\Delta m_J = 0$ transition matches the corresponding theoretical quantity. Exceptions to this are the experimental values for the polarization XY+XZ which were obtained with the polarization analyzer removed; the signal-to-noise ratio was somewhat higher and the intensities were determined by the area under the features.

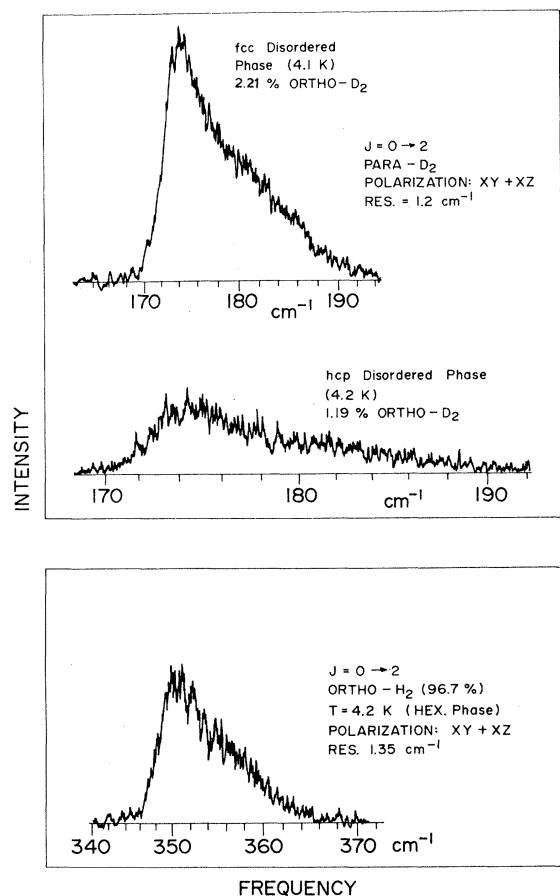


FIG. 18. $J=0 \rightarrow 2$ spectrum of small amounts of $J=0$ impurity molecules in the disordered phases of para- D_2 and ortho- H_2 ($T \approx 4.2$ K). For deuterium, spectra were recorded for both hcp and fcc orientationally disordered phases.

B. $J=1 \rightarrow 3$ spectrum

1. Disordered state

Figure 19 shows the $J=1 \rightarrow 3$ spectra observed in the disordered phases of paradeuterium. The spectrum for the hexagonal phase was taken before the sample was cooled below T_c and had $X=98.8\%$. The spectrum labelled cubic phase was taken after the sample had been cycled several times through the transition and therefore, according to the result of Schuch *et al.*,³² was predominantly in the cubic phase ($X=97.8\%$). This was corroborated by a disappearance of the hcp phonon.⁴⁶ We have plotted the logarithm of the intensity in order to emphasize the near exponential behavior of the high-frequency tail. (Above $\bar{\nu}=310$ cm^{-1} the intensity varies approximately as $e^{\bar{\nu}/a}$ where $a=6.25$ cm^{-1} .) In view of the analysis of the ordered-state spectrum presented in the following section, it is reasonable to conjecture that much of this tail is due to combinations in which a J

$=1 \rightarrow 3$ transition is accompanied by reorientations of neighboring $J=1$ molecules (the direct analog of the $J=1 \rightarrow 3$ roton plus libron transitions of the ordered phase). This accounts for the lack of a low-frequency tail since the temperature is considerably less than the bandwidth of the $J=1 \rightarrow 1$ orientational band. The higher frequency orientational modes are therefore not thermally populated. The present lack of a theory for the line shape precludes any quantitative analysis.

The corresponding $J=1 \rightarrow 3$ spectrum in the hexagonal disordered phase of orthohydrogen is shown in Fig. 20.

2. Ordered state

In the ordered state, one expects excitations from the nondegenerate $J=1$ ground state to the $J=3$ manifold to form a band with well-defined dispersion curves: E vs \vec{k} . As with the librions, one should see features corresponding to the $\vec{k}=0$ modes. Since there are a total of 27 possible modes [four lattice sites, and $(2J+1)=7$ states per site] one might expect a large number of lines, even allowing for some degeneracy. Therefore it was very puzzling when the spectrum was first observed,^{8,11} that there were only three features, each of a different width. Figure 21 shows the results obtained in the present experiment for the same oriented crystal used to obtain the libron spectra. The polarization analyzer has been removed to give maximum signal-to-noise. One again sees only three features: the lowest energy one having a width of about 1.5 cm^{-1} , only slightly larger than the instrumental width of 1.25 cm^{-1} , the central line being considerably broader (2.5 cm^{-1}), and the upper line having an enormous high-frequency tail of approximately exponential character.

When the spectra were obtained with the polarization analyzer in place, Figs. 22(a) and (b), differences in the relative mode intensities for the various polarizations XY , XZ , YY , YZ were evident. On later examination it was also noted that there were small frequency shifts and changes in line shape from one polarization to the next. This immediately suggested that each feature consisted of two or more unresolved lines of different symmetries. Since the polarization dependence of the modes depends on their symmetry, one could separate the modes in turn by appropriate linear combinations of the spectra. (The A_g modes are predicted to have zero Raman intensity.) The spectra of Figs. 22(a) and (b) are not very suitable for this procedure because of the compressed and somewhat erratic frequency scale. However, since the apparatus had been dismantled these

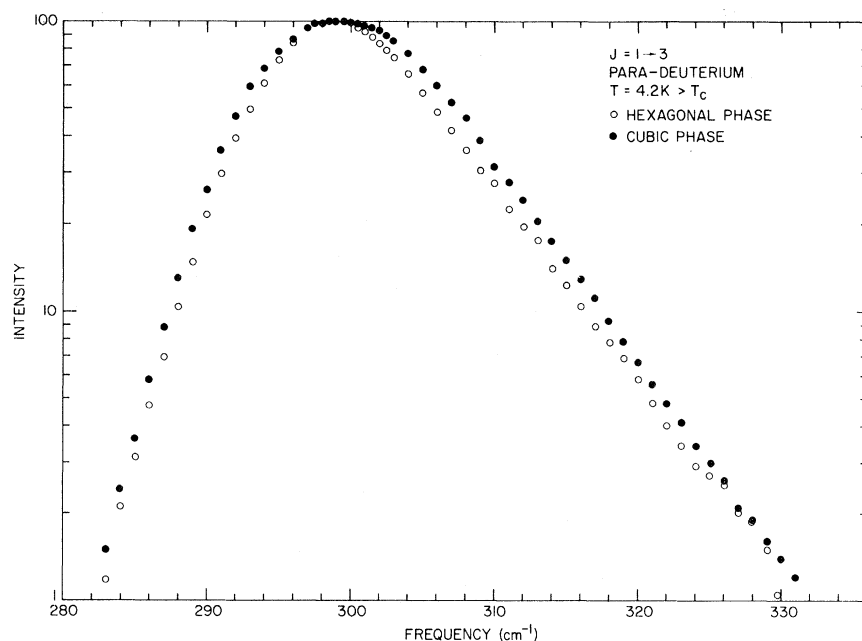


FIG. 19. $J=1 \rightarrow 3$ spectrum observed in both hcp and fcc disordered phases of high-purity para- D_2 at $T=4.2$ K. Purities were 98.8 and 97.8% for hcp and fcc spectra, respectively.

remained the only single-crystal data available on the $J=1 \rightarrow 3$ Raman transitions. Fortunately, by very careful processing of the data (see Appendix B) it was possible to convert the spectra to a common frequency scale and then to construct arbitrary linear combinations thereof.

In attempting to separate the modes we have made the assumption that the intensities of the E_g and T_g modes of the $J=1 \rightarrow 3$ spectrum have the same polarization dependencies as the respective libron modes. Since there was some uncertainty in the orientation of the crystal, we used the experimental values for the libron-mode intensities. To within the error involved this should permit complete separation. Accordingly, we have constructed linear combinations of the spectra corresponding to the mixture $XZ - 0.60XY$ which

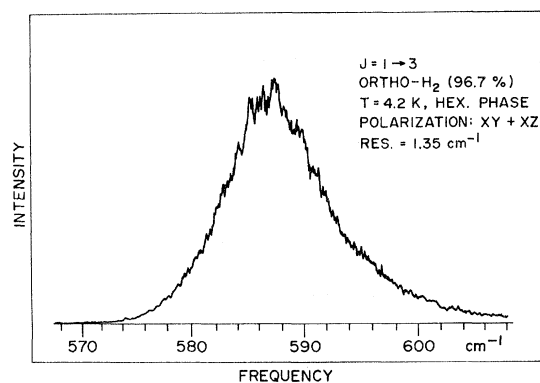


FIG. 20. $J=1 \rightarrow 3$ Raman spectrum of 96.7% ortho- H_2 in the hcp disordered phase ($T=4.2$ K).

should suppress all of the T_g modes, and the mixture $XY - 0.53XZ$ which should suppress all of the E_g modes. Similarly the mixture $YZ - 0.45YY$ suppresses T_g modes and $YY - 0.57YZ$ suppresses E_g modes. We have then averaged the two sets of pure E_g and pure T_g modes, and the results are shown in Fig. 23. The linear combinations quoted above are based on the experimental T_g and E_g libron-mode dependencies that were observed in the same crystal. It is doubtful that the E_g and T_g modes are completely separated in Fig. 23 since there was some uncertainty in the coefficients. However, the frequency shifts of the two lower features are easily discernible, and the relative intensities of the features are quite different. In passing we note that the broad upper feature seems to have predominantly T_g character. In Table V the absolute energies of the various transitions are listed, along with their values relative to the unperturbed $J=1 \rightarrow 3$ energy as determined experimentally from the Raman spectrum of 2% para- D_2 in ortho- D_2 (see Fig. 24). The detailed assignments are based on the theoretical results of Nakamura *et al.*³⁰ and Lee *et al.*⁴⁷ to be described in the following paragraphs, aided by the experimental separation of the E_g and T_g modes.

There have been two attempts to calculate the positions and intensities of the $J=1 \rightarrow 3$ roton lines. Lee, Raich, and Etters⁴⁷ based their treatment on Van Kranendonk's theory of energy bands in solid parahydrogen. This is a linear spin-wave type of theory and is expected to work well when the bandwidth to gap ratio is small. Their results,

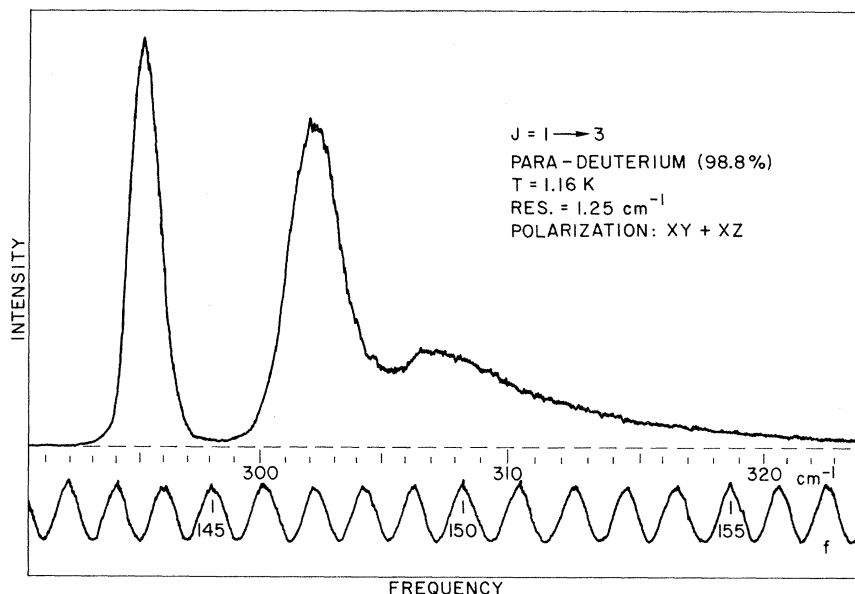


FIG. 21. $J=1 \rightarrow 3$ Raman spectrum observed in 98.8% para- D_2 in the low-temperature ordered phase.

for the case of EQQ interactions only and no crystal field, are given in Table VI. Also shown are the results of Nakamura, Miyagi and Fujio³⁰ who independently calculated the positions and intensities, and in addition labelled the mode symmetries. Their theory appears also to be a linear spin-wave treatment assuming pure EQQ interactions. Although the results are very similar to those of Lee *et al.*,⁴⁷ there are quantitative differences that become increasingly noticeable at the lower frequencies.

In the theoretical model of Lee *et al.*⁴⁷ the positions of the $J=1 \rightarrow 3$ Raman lines are given by

$$\epsilon_n = E_n + 38\Gamma/3 + E_0,$$

where E_n are the $k=0$ energy levels of the $J=3$ roton bands and E_0 is the energy of the unperturbed $J=1 \rightarrow 3$ transition. The term $38\Gamma/3$ is the nearest-neighbor molecular-field result for the difference in energy between the unperturbed $J=1$ level and the $J=1$ ground state. This shift becomes $42.4\Gamma/3$ when all neighbors are considered⁹ and in Table VI we have in fact reproduced values of $\epsilon_n - E_0 = E_n + 42.4\Gamma/3$, which can be compared directly to the experimental results of Table V. The theoretical energies of Nakamura *et al.*³⁰ are given directly in this form.

It is evident that with the assignments forced on us by the polarization dependencies, the correspondence between theory and experiment is generally poor. An exception to this is the separation and relative intensities of the two E_g modes, where the agreement is fair. The strong compression of the T_g modes is very reminiscent of the depression of the single-libron modes by the pre-

sence of the two-libron modes. If one postulates that the broad upper feature is a roton plus libron band with predominantly T_g character, then a consistent picture emerges: the E_g modes are little affected by the librations and their energies should therefore agree with theory (which neglects roton-libron coupling). One then has to account for the negative shift of about 5Γ of the two E_g modes. This may be due to an incorrect choice of E_0 , which was determined from the $J=1 \rightarrow 3$ spectrum of 2% para- D_2 in ortho- D_2 (Fig. 24), but such a large discrepancy seems unlikely. Although one would have preferred a smaller concentration of para- D_2 , the line is fairly narrow with the expected shoulders due to $J=1$ pairs. The value of E_0 so determined is 298.75 cm^{-1} , only slightly different from the gas-phase value of 297.5 cm^{-1} . There remains the possibility that E_0 is different for para- D_2 in ortho- D_2 than for pure para- D_2 . One possibility is the virtual excitations that do not conserve J . However, recent calculations⁴⁸ show that corrections to E_0 of this type amount to of order 1 cm^{-1} or less, and a considerable discrepancy still remains.

Lee *et al.*⁴⁷ and Nakamura *et al.*³⁰ also calculate the effect on roton energy levels of a crystalline field having a threefold symmetry axis. These results have not been included in Table VI since they afford no significant improvement in the agreement between theory and experiment.

For completeness, the $J=1 \rightarrow 3$ spectrum of 94.5% ortho- H_2 in the ordered state is shown in Fig. 25. No attempt was made to separate the modes as in D_2 .

It is clear from the present data that current

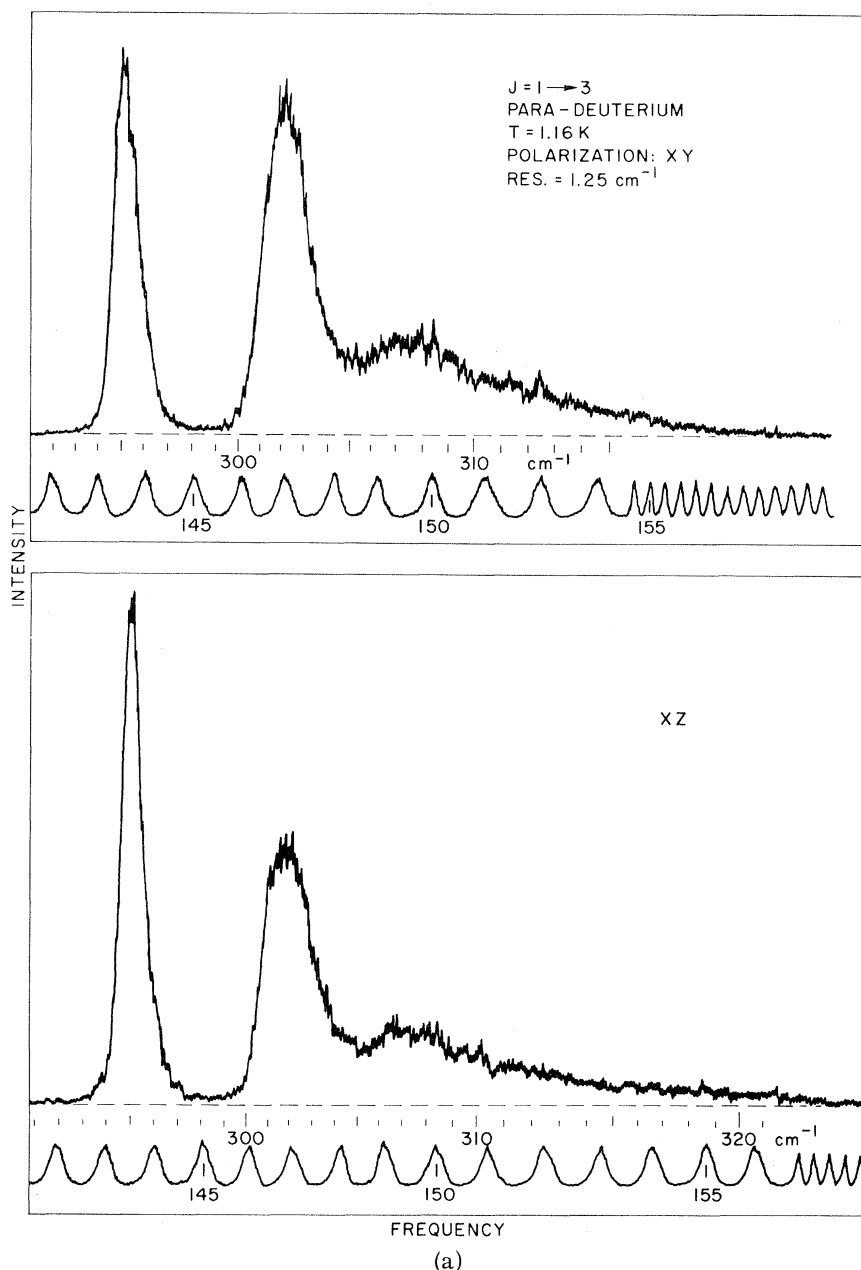


FIG. 22. $J=1 \rightarrow 3$ Raman spectrum in 98.8% para- D_2 in the ordered phase for (a) polarizations XY and XZ and (b) polarizations YY and YZ .

theories for the $J=1 \rightarrow 3$ roton band are inadequate. In view of the difficulties encountered in interpreting the libron data that remained unresolved until libron-libron interactions were included, it is not surprising that the simple roton theory is not very satisfactory. The problem is that there are accessible levels (the libron band) close to the ground state, and the conditions for success of the spin-wave-type theory are not satisfied. A solution to the coupled libron-roton problem unfortunately seems quite formidable. In the meantime, it

would be worthwhile repeating the present measurements at higher resolution.

V. MEASUREMENT OF ORTHO-PARA RATIO AND CONVERSION RATE

In this work the ortho-para ratio of the samples was determined spectroscopically from the relative intensities of the $J=0 \rightarrow 2$ and $J=1 \rightarrow 3$ rotational Raman transitions. Since there has not been an independent check of $I(J=0 \rightarrow 2)/I(J=1 \rightarrow 3)$ vs concentration X (by, for example, thermal-con-

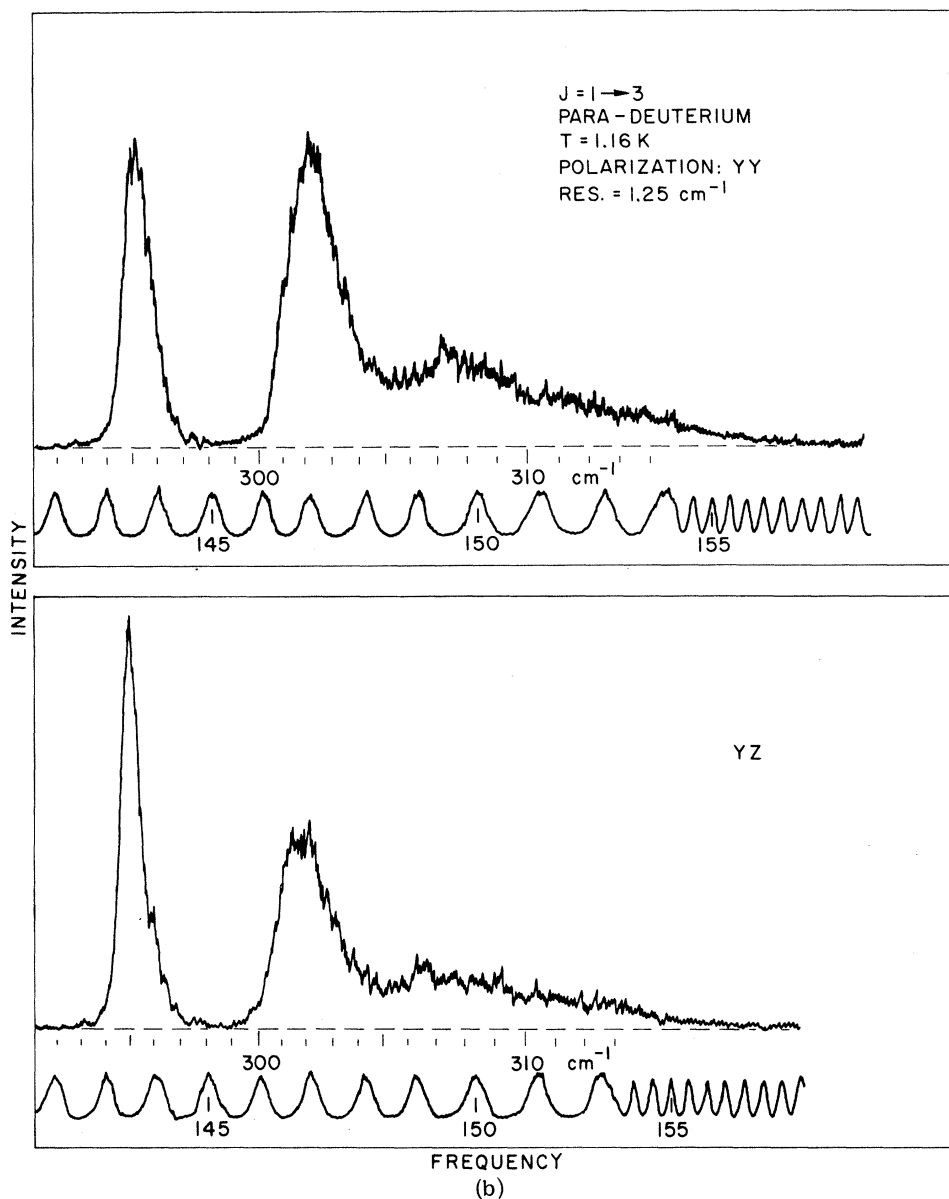


FIG. 22. Continued.

ductivity measurements on the gas) one has to rely on a theoretical calculation of the intensities. For a dilute gas, where one can treat the molecules as independent, and in addition ignore local-field effects, a straightforward calculation of the total Raman intensities (summing over final states and averaging over initial states) yields

$$I_{0 \rightarrow 2} / I_{1 \rightarrow 3} = \frac{2}{3} [c / (1 - c)] \quad (3)$$

Here $c = 1 - X$ is the concentration of $J = 0$ species and it has been assumed that there is no thermal population of the upper states. Previously¹¹ we had applied this result to the hcp phase of the solid, arguing that one only required orientational disorder to treat the molecules independently.

However, at 4 K where the measurements are normally made, there is considerable short-range order, i.e., correlation between orientations of neighboring molecules, and it seems unlikely that the result holds exactly. Indeed, it is possible to set up the calculation for the solid in terms of moments of the polarizability operator. If one assumes a pure EQQ intermolecular interaction one can evaluate the moments in terms of a high-temperature expansion. Unfortunately such expansions are known to converge very slowly⁴⁹ and would not be reliable in the present case at 4.2 K, although an examination of the leading terms seemed to indicate deviations from Eq. (3). Since some important aspects of the present work

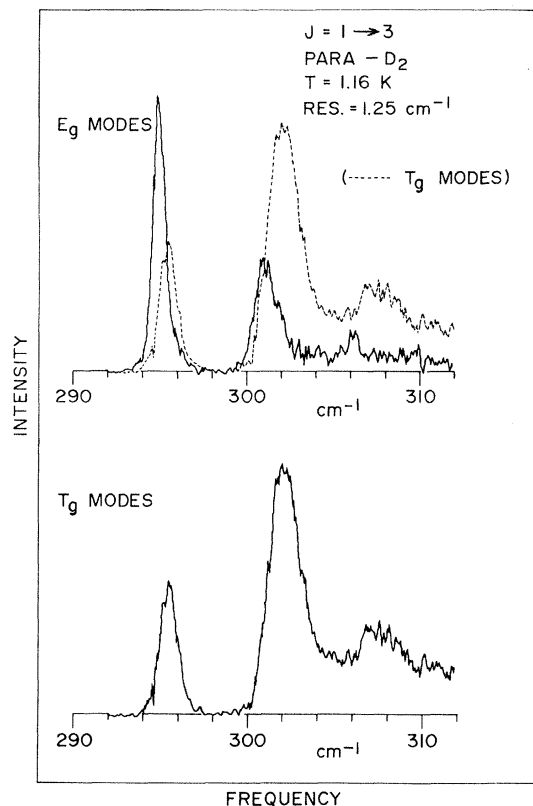


FIG. 23. Computer print out of linear combinations of the processed spectra of Fig. 22. The linear combination for the upper solid trace has been arranged to suppress T_g modes, leaving only E_g modes, whereas the reverse is true for the bottom solid line. The dotted line, a replica of the pure T_g spectrum, is included so that the shifts of the lines are more easily seen.

depend critically on an accurate knowledge of c , we looked for other ways to check the $\frac{5}{3}$ factor in Eq. (3). Although in principle we could determine the concentration independently from the measured transition temperature by using the results of Schuch *et al.*,³ the accuracy was not sufficiently high in general. The most accurate check on Eq. (3) came indirectly from a measurement of $I_{0 \rightarrow 2}/I_{1 \rightarrow 3}$ as a function of time. By applying Eq. (3) one can deduce conversion rates (see Fig. 26) which can then be compared to other independent measurements. The comparison is made in Table VII and one notes remarkably good agreement. Hence it seems that the $\frac{5}{3}$ prefactor can be used with moderate confidence.

In looking for internal consistency we have also measured $I_{1 \rightarrow 1}/I_{1 \rightarrow 3}$, where $I_{1 \rightarrow 1}$ is the intensity of the feature near zero frequency (in the ordered state this is the libron band), and compared the result to theory⁵³ (Table VIII). The calculation for the disordered phase is based on no short-

TABLE V. Frequency shifts of the $J = 1 \rightarrow 3$ features in the Raman spectrum of ordered para- D_2 for $X = 0.985$ and $T = 1.16$ K.

Mode	$\bar{\nu}$ (cm^{-1})	$\Delta\bar{\nu}^a$ (cm^{-1})	Units of Γ^b
$E_g^{(1)}$	294.95	-3.80	-4.74
$T_g^{(1)} + T_g^{(2)}$	295.47	-3.28	-4.09
$E_g^{(2)}$	301.25	+2.50	3.12
$T_g^{(3)} + ?$	302.32	+3.57	4.45

^a Energy origin = 298.75 cm^{-1} as taken from $J = 1 \rightarrow 3$ spectrum of 2% para- D_2 in ortho- D_2 (Fig. 24).

^b Γ_0 is taken to be 0.802 cm^{-1} , the value derived from the libron spectra.

range order. The reasonably small difference between theory and experiment shows that the relative intensities are not greatly affected by short-range order, and indirectly lends further support to the use of Eq. (3).

VI. DISCUSSION

The current level of understanding of the ground state in the orientationally ordered phase of para-deuterium and orthohydrogen and the low-lying excitations—the librons—appears to be excellent. The situation for the higher-energy rotational excitations (with $\Delta J \neq 0$) is less satisfactory although a reasonably consistent picture can be constructed, the details of which, however, will require a considerable amount of further theoretical work. It has turned out, perhaps somewhat surprisingly, that the librons interact very strongly with the higher rotational excitations, producing large energy-level shifts and combination bands. A thorough understanding of the librons, and especially the effects of anharmonicity seems now to be crucial to a proper description of these higher rotational modes. Furthermore, such an understanding is required to describe the effects of $J = 0$ impurities, temperature, and density on the properties of the ordered phase.

Present experimental data on the one- and two-libron Raman transitions show very good agreement with anharmonic theories based on the Pa3 structure and a renormalized EQQ interaction involving a single parameter Γ_{eff} . The value of Γ_{eff} deduced from the $\vec{k} = 0$ librons has been brought into even better agreement with other measurements by the recent work of Harris *et al.*¹⁹ who took into account the effect of virtual $J = 3$ processes. In lowest order this produces a common energy shift of the libron modes and hence changes the value of Γ_{eff} . At this point, a calculation of

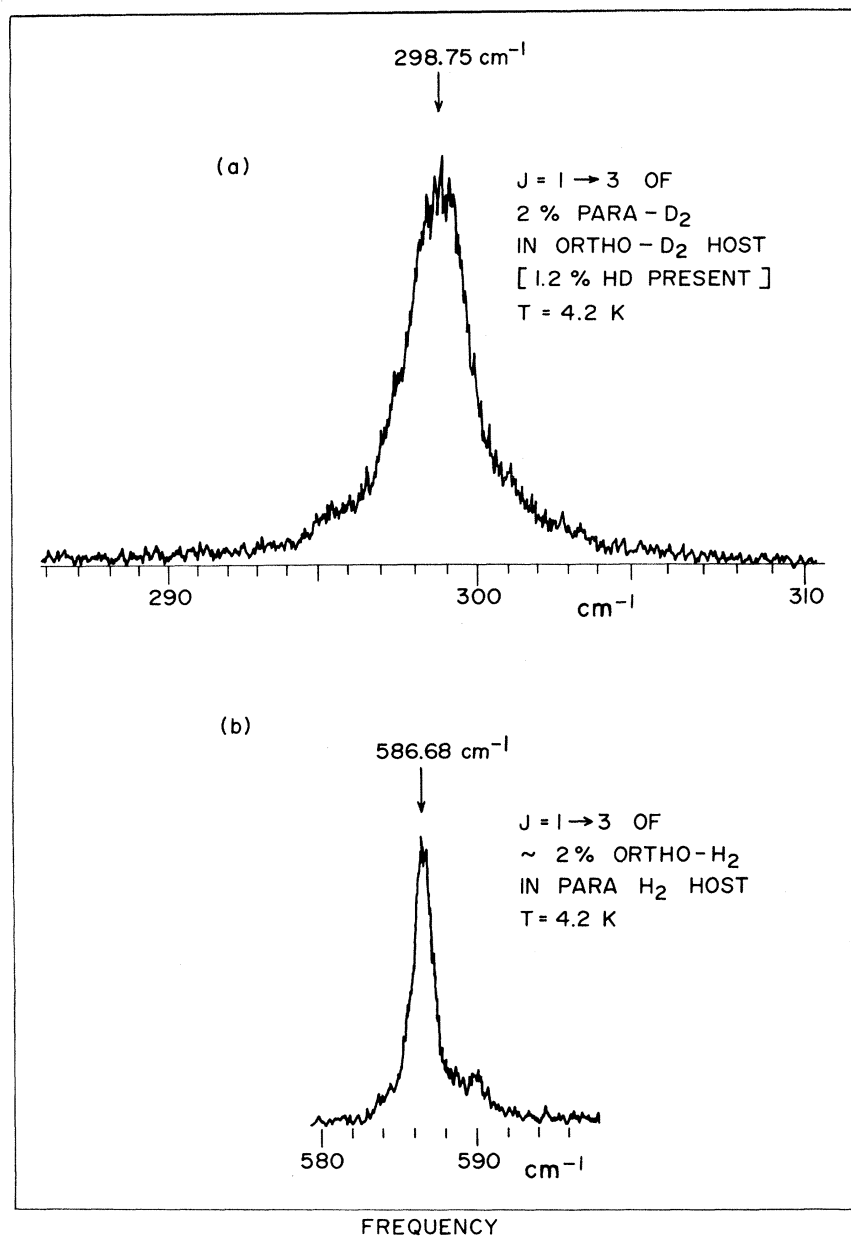


FIG. 24. Raman spectrum of small amounts of $J=1$ molecules in $J=0$ hosts for both H_2 and D_2 . These spectra are used to determine the effective rotational constant in the solid.

the shift for each of the libron modes seems important, especially for para- D_2 where the effect is large, of order 10%. The most recent work of Fujio and Nakamura³⁰ appears to have reached this objective, but now the agreement with experiment is less satisfactory. A quantitative understanding of these polarization effects will be particularly critical in the interpretation of high-pressure libron frequencies since the relative importance of the shift varies as Γ/B .

Any complete understanding of the dynamics of the ordered state will require confirmation of the libron dispersion relationship. The present one-

libron Raman lines only provide detailed information about the zone center, while the two-libron band, which involves librations of equal and opposite \vec{k} , probes other parts of the Brillouin zone, especially the zone edges. However, the information obtained in the latter case is not as useful as that obtained from coherent inelastic neutron scattering which in principle gives the dispersion curves directly. Unfortunately, the possibility of such measurements seems remote because of the small form factor and the bothersome ortho-para conversion.⁵⁴ On the other hand, the one-libron density of states can be obtained with quite good re-

TABLE VI. Comparison of observed $J=1 \rightarrow 3$ features in para- D_2 with theoretical $\bar{k}=0$ roton modes ($X=0.985$, $T=1.16$ K). The energies are measured relative to the unperturbed $J=1 \rightarrow 3$ transition.

Mode	E/Γ			Intensity		
	LRE ^a	NMF ^b	Expt. ^c	LRE ^a	NMF ^b	Expt. ^d
A_g	-6.53	-9.00	...	0	0	...
$T_g^{(1)}$	-1.34	-1.90	(-4.09) ^e	0.14	0.35	(1.24) ^e
$E_g^{(1)}$	-0.20	-0.95	-4.74	1	1	1
$T_g^{(2)}$	0.14	0.05	(-4.09) ^e	0.039	...	(1.24) ^e
$E_g^{(2)}$	8.74	9.00	3.12	0.80	1.11	0.92
$T_g^{(3)}$	14.21	13.10	4.45	1.53	2.67	3.70
$T_g^{(4)}$	24.17	23.8
$T_g^{(5)}$	25.36	25.4
$A_g + T_g + 2E_g$	24.69	25.9	...	0

^aLee, Raich, and Eiters (Ref. 46); the quantity 42.4/3 corresponding to the depression of the $J=1$ ground state has been added in order to compare their results to Nakamura *et al* (Ref. 30) and to experiment.

^bNakamura, Miyagi, and Fujio (Ref. 30).

^c Γ is taken to be 0.802 cm^{-1} , the value derived from the libron spectra.

^dThese are equivalent intensities for a powder sample derived by assuming the angular dependencies to be the same as for librions of equivalent symmetry. See Appendix A.

^eThe $T_g^{(1)}$ and $T_g^{(2)}$ modes are not resolved and the common values correspond to the center of the single feature observed.

solution from *incoherent* neutron scattering.⁵⁵ Optical measurements of the two-libron band, with high enough signal to noise and resolution that the singularities in the spectrum can be detected, will also provide detailed information on libron dynamics. Furthermore, a comparison of the two-libron optical spectrum with the one-libron neutron spectrum is a sensitive probe of libron-libron interactions.

In this paper we have presented the temperature and concentration dependence of several libron

parameters. In general, there are no theories with which to compare the experimental results, and we have therefore presented the data in reduced forms, pointing out some suggestive systematics in hopes of stimulating further theoretical work. For the case of the libron frequencies, it was useful to compare their temperature dependence with experimentally determined values of the order parameter which, in the RPA approximation at least, is proportional to the libron frequencies. The result was that the librions seemed

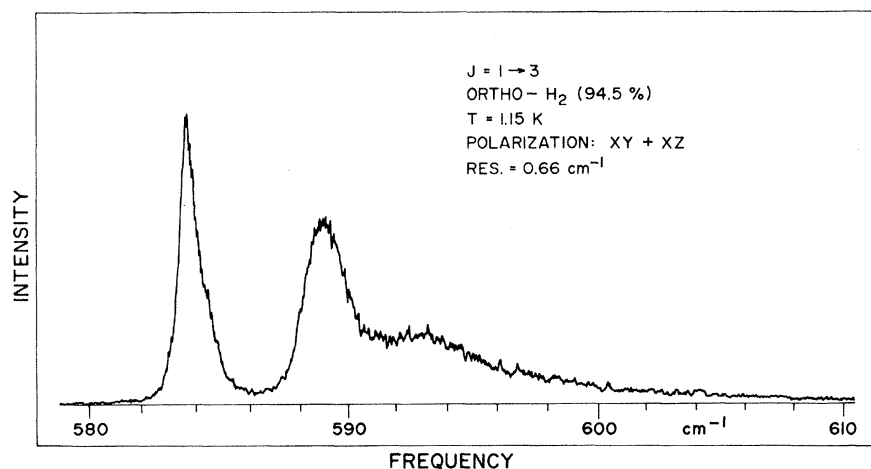


FIG. 25. $J=1 \rightarrow 3$ Raman spectrum of 94.5% ortho- H_2 in the low-temperature ordered state.

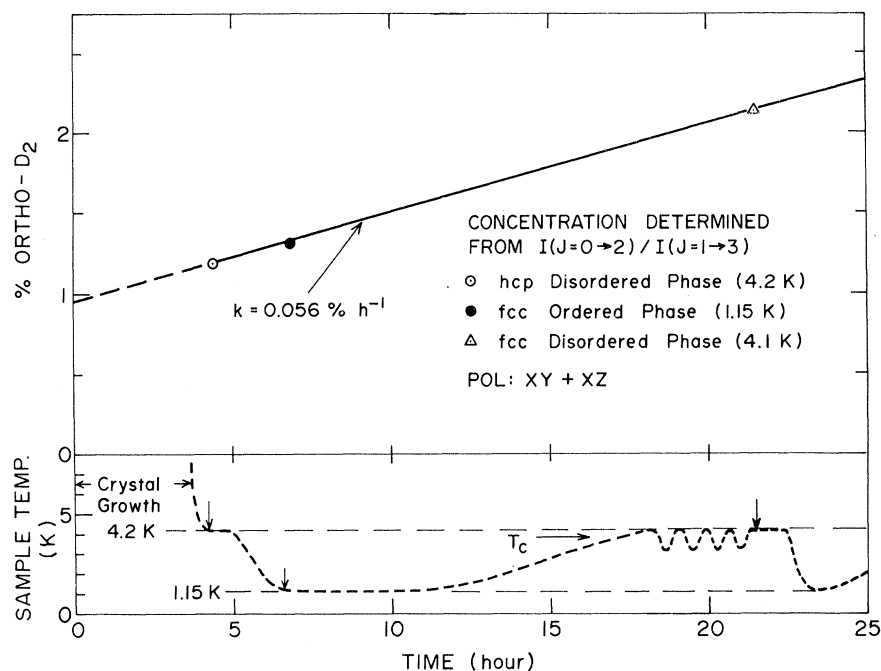


FIG. 26. Time dependence of the ortho- D_2 concentration in solid para- D_2 . Also shown is the thermal history of the sample.

to have a weaker temperature dependence than the order parameter. Libron linewidths were also studied and the temperature broadening fitted to an exponential in $1/T$. Here again there is a lack of published theory.

Measurements of the libron frequencies as a function of $J=0$ impurity concentrations point out the inadequacy of the molecular-field theories; a comparison of the present results with specific-heat data seems to show that the concentration dependence is different for librions of differing \vec{k} .

There is a similar situation, with regard to lack of theory, for the $J=0 \rightarrow 2$ transition of the impurity molecules for both the ordered and disordered phases. We have concluded, in agreement with Boggs *et al.*,⁴⁵ that the highest-frequency feature is a libron sideband, and have further speculated that the large shifts in frequencies from the molecular-field values are due to coupling with the librions.

The complete inadequacy of current theory to explain the observed $J=1 \rightarrow 3$ features in the ordered state is presumably related to the use of an exciton theory whose success depends on the existence of a nondegenerate ground state well separated from the excited states (as in the case for example in the $J=0 \rightarrow 2$ roton bands in para-hydrogen).^{41,56} Although in the present case the ground state is nominally nondegenerate, there is a band of states nearby, namely, the librions, that are strongly coupled to the exciton modes, and this greatly complicates the situation. It seems clear that in addition to further theoretical work,

experiments at higher resolution and sample purity will be required to resolve this problem.

ACKNOWLEDGMENTS

The authors would like to thank Lloyd Ahlberg and John Curnow for their expert technical assistance throughout the experimental work, and Wayne Norris for developing the computer programs used in the data analysis. They are indebted to A. J. Berlinsky for several stimulating discussions and also for assistance in calculating some of the Raman intensities. They thank Professor T. Nakamura for communicating certain

TABLE VII. Conversion rates in solid ortho- H_2 and para- D_2 for $T \leq 4.2$ K. There is no evidence for the conversion rates being different for the ordered and disordered state. The rates given above are for samples having a nominal purity of 100% $J=1$ species.

Conversion Rate ($\% h^{-1}$)	
H_2	
This work	1.88
Jarvis <i>et al.</i> ^a	1.85
D_2	
This work	0.056
Weinhaus <i>et al.</i> ^b	0.057
Grenier and White ^c	~ 0.1

^aReference 50.

^bReference 51.

^cReference 52.

TABLE VIII. Experimental ratios of total Raman intensities (polarization $XY+XZ$) between the $J=1 \rightarrow 1$ and $J=1 \rightarrow 3$ pure rotational transitions in solid para-deuterium. The values given in parentheses are derived from the approximate theory discussed in the text.

Time (h)	Temp. (K)	Phase	$\frac{I(1 \rightarrow 3)}{I(1 \rightarrow 1)}$	$\frac{I(0 \rightarrow 2)}{I(1 \rightarrow 3)}$	Inferred $o\text{-D}_2$ concentration (%)
4.42	4.2	hcp disord.	1.69(1.875)	0.020	1.19
6.87	1.16	fcc ord.	1.41(1.45)	0.022	1.32
21.5	4.1	fcc disord.	1.65(1.875)	0.0376	2.14

results prior to publication. One of the authors (I.F.S.) thanks the "Stichting voor Fundamenteel Onderzoek der Materie" for partial financial support. J.P.M. was partially supported by a grant from the National Science Foundation, and W.N.H. was partially supported by the National Research Council of Canada.

APPENDIX A: CALCULATION OF RAMAN INTENSITIES

The simplest way to calculate rotational Raman-scattering intensities in molecular solids is to apply the standard polarizability approximation used for isolated molecules,⁵⁷ the polarizability now being the sum of the individual molecular polarizabilities. The wavelength of the light is no longer large compared to the dimensions of the scattering center, but proper treatments of the scattering process⁵⁸ show that for many practical purposes one can assume the wavelength of the light to be infinite and therefore uniform across the sample, and the excitation from which it scatters to be at $k=0$. There is the further problem that the dipoles induced by the incident radiation interact with their polarizable neighbors which is clearly an effect that increases with $\epsilon - 1$, where ϵ is the dielectric constant of the solid. For hydrogen ($\epsilon \approx 1.3$) the effect is expected to be small and will be ignored.

The calculations that follow constitute a detailed account of results used previously in the analysis of Raman spectra,^{9,11,18} and provide a basis for comparing present Raman results with theory. They also show explicitly, for the first time, the correspondence between the libron scattering matrices and the standard scattering matrices given by Loudon⁵⁹ for the *vibrational* modes of cubic crystals. Some of the results have also been derived by Nakamura and Miyagi,²⁹ in particular the polarization dependencies of the scattered light for the libron modes; their calculations were based on a harmonic model, whereas the present results are derived from the Bloch spin-wave approximation.⁷ The sophisticated and formally more correct calculations of Coll and Harris^{13,16} for libron intensities in various harmonic and anharmonic approximations have been restricted

to powder samples and therefore give only total mode intensities. They will be used in conjunction with our own results to compare theory to data obtained in single crystals.

Consider the scattering geometry in Fig. 3 where light of polarization $\vec{\sigma}$ and frequency ω_0 is incident along the z direction, and the component of scattered light having polarization \vec{p} is detected in the x direction. Following Wilson *et al.*,⁵⁷ the power emitted per unit solid angle per unit frequency due to scattering in which the physical system changes from state $|i\rangle$ to $|j\rangle$ is given by

$$I^{\sigma p}(i \rightarrow j) = 4[(\omega_0 - \omega_s)/c]^4 n_i \times I_0 |\langle i | \alpha_{\sigma p} | j \rangle|^2 \delta(\omega_s - \omega_{ij}), \quad (\text{A1})$$

where ω_s is the frequency shift of the scattered light, $\omega_{ij} = \hbar^{-1}(E_j - E_i)$ the frequency of the transition, c the velocity of light, n_i the thermal population factor of the initial state, and I_0 the intensity (power/unit area) of the incident light. Here the quantity $\alpha_{\sigma p}$ is a Cartesian component of the total polarizability tensor: $\underline{\alpha} = \sum_{p=1}^N \underline{\alpha}(p)$, where $\underline{\alpha}(p)$ is the polarizability tensor of the p th molecule and N the total number of molecules.

Since for the situations we wish to consider the states $|i\rangle$ and $|j\rangle$ are expressed in terms of products of spherical harmonics, it is convenient to also write the Cartesian components of $\underline{\alpha}$ for a single molecule in terms of spherical harmonics. In the principal-axis frame of a diatomic molecule (z direction along internuclear axis) with $\alpha_{xx} = \alpha_{yy} = \alpha_{\perp}$ and $\alpha_{zz} = \alpha_{\parallel}$, then for any vector \vec{E} the quantity $\vec{E} \cdot \underline{\alpha} \cdot \vec{E}$ is given by

$$\begin{aligned} \vec{E} \cdot \underline{\alpha} \cdot \vec{E} &= E^2(\alpha_{\perp} \sin^2 \theta + \alpha_{\parallel} \cos^2 \theta) \\ &= E^2 \left[\frac{1}{3}(2\alpha_{\perp} + \alpha_{\parallel}) + \frac{1}{3}(\alpha_{\parallel} - \alpha_{\perp}) \right. \\ &\quad \left. \times (3 \cos^2 \theta - 1) \right], \end{aligned} \quad (\text{A2})$$

where θ is the angle between \vec{E} and the z axis. Ignoring from now on the isotropic part of $\underline{\alpha}$ which makes no contribution to libron and rotational scattering processes, and transforming to a general coordinate frame using the spherical-harmonic addition theorem,

$$\vec{E} \cdot \underline{\alpha} \cdot \vec{E} = \frac{8}{15} \pi (\alpha_{\parallel} - \alpha_{\perp}) E^2 \sum_{m=-1}^{+1} Y_{2m}^*(\Omega_M) Y_{2m}(\Omega_E). \quad (\text{A3})$$

Here Ω_M and Ω_E are the spherical coordinates of the molecular axis and the vector \vec{E} , respectively, expressed in the general frame. Evaluating both sides for specific directions of \vec{E} , the Cartesian components of $\underline{\alpha}$ are obtained:

$$\begin{aligned} \alpha_{XZ} &= \Delta(Y_{21} - Y_{2-1}), & \alpha_{YZ} &= -i\Delta(Y_{21} + Y_{2-1}), \\ \alpha_{XY} &= i\Delta(Y_{2-2} - Y_{22}), & \alpha_{ZZ} &= \left(\frac{8}{3}\right)^{1/2} \Delta Y_{20}, \\ \alpha_{YY} &= -\Delta\left[\left(\frac{2}{3}\right)^{1/2} Y_{20} + Y_{22} + Y_{2-2}\right], \\ \alpha_{XX} &= \Delta\left[-\left(\frac{2}{3}\right)^{1/2} Y_{20} + Y_{22} + Y_{2-2}\right]. \end{aligned} \quad (\text{A4})$$

The argument of the Y_{2m} 's is understood to be Ω_M , and $\Delta = \left(\frac{2}{15}\pi\right)^{1/2} (\alpha_{\parallel} - \alpha_{\perp})$.

$$\langle J', m'_J | Y_{2m} | J, m_J \rangle = (-1)^{m'_J} \left(\frac{5(2J'+1)(2J+1)}{4\pi} \right)^{1/2} \begin{bmatrix} J' & 2 & J \\ 0 & 0 & 0 \end{bmatrix} \begin{bmatrix} J' & 2 & J \\ -m'_J & m' & m_J \end{bmatrix}, \quad (\text{A6})$$

where the bracketed expressions are Wigner 3- j symbols.⁶⁰ The results for a single molecule with the Cartesian z axis along the molecular-field axis are

$$\begin{aligned} \langle 0, 0 | \underline{\alpha}(\rho) | 2, 0 \rangle &= \left(\frac{2}{3}\right)^{1/2} \frac{\Delta}{(4\pi)^{1/2}} \begin{bmatrix} -1 & 0 & 0 \\ 0 & -1 & 0 \\ 0 & 0 & 2 \end{bmatrix}, \\ \langle 0, 0 | \underline{\alpha}(\rho) | 2, \pm 1 \rangle &= \frac{\Delta}{(4\pi)^{1/2}} \begin{bmatrix} 0 & 0 & \pm 1 \\ 0 & 0 & i \\ \pm 1 & i & 0 \end{bmatrix}, \\ \langle 0, 0 | \underline{\alpha}(\rho) | 2, \pm 2 \rangle &= \frac{\Delta}{(4\pi)^{1/2}} \begin{bmatrix} 1 & \pm i & 0 \\ \pm i & -1 & 0 \\ 0 & 0 & 0 \end{bmatrix}. \end{aligned} \quad (\text{A7})$$

For the oriented crystals used in the present experiments, one quarter of the sites in the cubic $Pa3$ phase have the molecular field in the laboratory z direction, whereas the rest are inclined at an angle θ_0 , where $\cos\theta_0 = \frac{1}{3}$. The intensities have therefore to be averaged over the different sites. Denoting the laboratory coordinate system by XYZ , the molecular-field frame by $X'Y'Z'$, and ϕ and θ the first two Euler angles in taking XYZ into $X'Y'Z'$ (θ is a rotation about the X' direction, see Fig. 3), then the components of \hat{e}_i and \hat{e}_s in the $X'Y'Z'$ molecular-field frame are given by

$$\hat{e}_i = \begin{bmatrix} \cos\delta \cos\phi + \sin\delta \sin\phi \\ -\cos\delta \cos\theta \sin\phi + \sin\delta \cos\theta \cos\phi \\ \cos\delta \sin\theta \sin\phi - \sin\delta \sin\theta \cos\phi \end{bmatrix} \quad (\text{A8})$$

In the circumstance that the Cartesian components of the total polarizability $\underline{\alpha}$ are known in a reference frame fixed in the crystal, then if the incident and scattered photons have polarizations in the directions of the unit vectors \hat{e}_i and \hat{e}_s , respectively, Eq. (1) can be expressed as⁵⁹

$$I^s(i \rightarrow j) = A \left| \sum_{\sigma, \rho = x, y, z} e_i^\sigma \langle i | \alpha_{\sigma\rho} | j \rangle e_s^\rho \right|^2, \quad (\text{A5})$$

where

$$A = 4[(\omega_0 - \omega_s)/c]^4 n_i I_0 \delta(\omega_s - \omega_{ij}).$$

Intensity of $J=0 \rightarrow 2$ for isolated $J=0$ impurity molecules in the fcc ordered phase

Denoting the states of the molecule by $|J, m_J\rangle$, the required matrix elements are found using Eq. (4) and

$$\hat{e}_s = \begin{bmatrix} \sin\epsilon \sin\phi \\ \sin\epsilon \cos\theta \cos\phi + \cos\epsilon \sin\theta \\ -\sin\epsilon \sin\theta \cos\phi + \cos\epsilon \cos\theta \end{bmatrix},$$

where δ is the angle between \hat{e}_i and the X direction, and ϵ the angle between \hat{e}_s and the Z direction. The intensities for specific values of δ , ϵ , and θ can then be easily evaluated using Eq. (5). For $\theta=0$ there is no ϕ dependence. For $\theta=\theta_0$ the ϕ dependence disappears when the intensities are summed over the three azimuthal angles of Z' that occur in a single crystallite: $\phi = \phi_0, \phi_0 + \frac{2}{3}\pi, \phi_0 + \frac{4}{3}\pi$. The final results, appropriately averaged over the two kinds of sites, are given in Table IV (main text) along with the experimental values. Also included for comparison are the results for a powder sample.

The reason for the imaginary quantities appearing in the polarizability matrices for $m_J = \pm 1$ and $m_J = \pm 2$, is that the basis functions Y_{lm} are complex. However, any orthonormal set can be used without changing the results, since the intensities have to be averaged over all degenerate states. It follows that for the purposes of calculating intensities, a set of polarizability matrices A^i , $i = 1, 2, \dots, n$, belonging to an n -fold degenerate transition can be replaced by any set of real matrices $B^i = \sum_j C_{ji} A^i$, provided that $\sum_{i,j} |C_{ij}|^2 = 1$.

Libron intensities in the $Pa3$ structure

For the calculation of the intensities, the linear spin-wave results of Mertens, Biem, and Hahn⁷ will be used. Although the Bloch spin-wave approximation is not particularly good for prediction

of the libron energies,^{7,15} the resulting eigenvectors have the correct symmetry and therefore yield the correct polarization properties of the scattered light. An advantage of this formalism is its conceptual simplicity.

$$\langle 0 | \underline{\alpha} | \vec{k}=0 \rangle = \left\langle \prod_{\vec{n}, g} \phi_g^0(\vec{n}, g) \left| \sum_{\vec{p}=1}^N \alpha(\vec{p}) \right| \frac{1}{\sqrt{N}} \sum_{\vec{m}, h} \sum_{\alpha} C_h^\alpha \prod_{\vec{0}, f \neq \vec{m}, h} \phi_f^0(\vec{0}, f) \phi_h^\alpha(\vec{m}, h) \right\rangle. \quad (\text{A9})$$

The state $\phi_g^0(\vec{n}, g)$ denotes the $m_J=0$ molecular-field ground state of a molecule at lattice position (\vec{n}, g) , where \vec{n} is a cubic translation vector and g labels the sublattice ($g=0, 1, 2, 3$). The state $\phi_h^\alpha(\vec{m}, h)$ denotes the $m_J=+1$ ($\alpha=+$) or $m_J=-1$ ($\alpha=-$) excited state of a molecule at position (\vec{m}, h) , and C_h^α gives the amplitude of ϕ_h^α for the libron mode of interest. A normalization factor $1/\sqrt{N}$ has been added so that $\langle \vec{k} | \vec{k} \rangle = 1$. Using the orthogonality of the states, Eq. (9) reduces to

$$\begin{aligned} \langle 0 | \underline{\alpha} | \vec{k}=0 \rangle &= \frac{1}{\sqrt{N}} \sum_{\vec{m}, h} \sum_{\alpha} C_h^\alpha \langle \phi_h^0(\vec{m}, h) | \underline{\alpha}(\vec{m}, h) \\ &\quad \times | \phi_h^\alpha(\vec{m}, h) \rangle \\ &= \frac{\sqrt{N}}{4} \sum_h \sum_{\alpha} C_h^\alpha \langle \phi_h^0 | \underline{\alpha}^h | \phi_h^\alpha \rangle, \quad (\text{A10}) \end{aligned}$$

where $\phi_h^\alpha = \phi_h^\alpha(\vec{q}, h)$ and \vec{q} is some arbitrary origin in the crystal. In order to evaluate matrix elements such as $\langle \phi_h^0 | \alpha_{XZ}^h | \phi_h^\alpha \rangle$ in which α_{XZ}^h is expressed in the laboratory frame and ϕ_h^0, ϕ_h^α are expressed in the sublattice frame h , either ϕ_h^0

The Raman intensity for the creation of a libron having wave vector $\vec{k}=0$ is determined by the absolute value squared of the matrix element $\langle 0 | \underline{\alpha} | \vec{k}=0 \rangle$, where $|0\rangle$ is the ground state. Using the notation of Mertens *et al.*,⁷

and ϕ_h^α have to be transformed to the lab frame or α_{XZ}^h to the h frame. We choose to do the latter, making the transformation in two steps, first from the lab frame to the cubic crystal frame, and then to the h frame. Taking as an example

$$\alpha_{XZ}^h = \Delta [Y_{21}(\Omega_i^h) - Y_{2-1}(\Omega_i^h)],$$

where Ω_i^h denotes the spherical coordinates of the molecule in the lab coordinate system, and using the convention of Rose⁶¹ for the rotation matrices,

$$\begin{aligned} \alpha_{XZ}^h &= \Delta \sum_m [D_{m1}^2(l) - D_{m-1}^2(l)] \\ &\quad \times \sum_{m'} D_{mm'}^{2*}(h) Y_{2m'}(\Omega_h^h), \quad (\text{A11}) \end{aligned}$$

where (l) denotes the Euler angles to rotate the cubic crystal frame into the laboratory frame, and (h) the Euler angles to rotate the crystal frame into the h frame. Ω_c^h and Ω_h^h are the spherical coordinates of molecule h in the crystal and h frames, respectively. Noting that $\phi_h^0 = Y_{10}(\Omega_h^h)$ and $\phi_h^\pm = Y_{1\pm 1}(\Omega_h^h)$, and using Eq. (6) to evaluate the matrix elements, one obtains

$$\begin{aligned} \langle 0 | \alpha_{XZ} | \vec{k}=0 \rangle &= -\frac{\sqrt{N}}{4} \Delta \frac{8\sqrt{3}}{5!} \left(\frac{45}{4\pi}\right)^{1/2} \sum_m [D_{m1}^2(l) - D_{m-1}^2(l)] \sum_{\alpha, h} D_{m-\alpha}^{2*}(h) C_h^\alpha \\ &= -K \sum_m [D_{m1}^2(l) - D_{m-1}^2(l)] P_m, \quad (\text{A12}) \end{aligned}$$

where $K = \frac{1}{5} (135N)^{1/2} \Delta$ and

$$P_m = \sum_{\alpha, h} D_{m-\alpha}^{2*}(h) C_h^\alpha.$$

For a powder sample one needs to average $|\langle 0 | \alpha_{XZ} | \vec{k}=0 \rangle|^2$ over all orientations of the crystal axes with respect to the lab axes. Using the orthogonality properties of the D 's [Rose (Ref. 61), p. 75], one obtains

$$\begin{aligned} |\langle 0 | \alpha_{\sigma\rho} | \vec{k}=0 \rangle|^2 &= \frac{2}{5} K^2 \sum_m |P_m|^2 \quad \text{for } \sigma \neq \rho \\ &= \frac{8}{15} K^2 \sum_m |P_m|^2 \quad \text{for } \sigma = \rho. \quad (\text{A13}) \end{aligned}$$

The eigenvectors

$$\vec{c} = \begin{bmatrix} c^+ \\ c^- \end{bmatrix}$$

for $\vec{k}=0$ are easily obtained from the results of Mertens *et al.*⁷ and are given in Table IX. There are six circularly polarized modes labelled (c, ia) , (c, ib) , where $i=1, 2, 3$, and two longitudinal modes labelled $(l, 1)$ and $(l, 2)$.

The Euler angles for the transformations from the cubic to h frames are given in Table X along with the conventions used for the Z and X directions in each coordinate system. In Table XI are given the $d_{m'm}^{2*}(\beta)$ [generated by the prescription given by Edmonds (Ref. 60, p. 62), and converted to Rose's⁶¹ convention: $d_{m'm}^{2*}(\beta) (\text{Rose}) = (-1)^{m'-m}$

TABLE IX. Eigenvectors for $\vec{k}=0$ libron modes.

$T_g : E/\Gamma = 19 + R + 2 A $		$\epsilon = e^{i2\pi}, \eta = e^{i\kappa} = A/ A $	
$\vec{C}(c, 1a) = \frac{1}{\sqrt{6}}$	3 2 $\epsilon\eta^*$ 2 $\epsilon^*\eta^*$ 2 η^* 0 ϵ ϵ^* 1	$\vec{C}(c, 1b) = \frac{1}{\sqrt{6}}$	0 ϵ^* ϵ 1 3 2 $\epsilon^*\eta$ 2 $\epsilon\eta$ 2 η
$\vec{C}(l, 1) = \sqrt{\frac{2}{3}}$			0 η^* η^* η^* 0 - η - η - η
$T_g : E/\Gamma = 19 + R - 2 A $			
$\vec{C}(c, 2a) = \frac{1}{\sqrt{6}}$	3 -2 $\epsilon\eta^*$ -2 $\epsilon^*\eta^*$ -2 η^* 0 ϵ ϵ^* 1	$\vec{C}(c, 2b) = \frac{1}{\sqrt{6}}$	0 ϵ^* ϵ 1 3 -2 $\epsilon^*\eta$ -2 $\epsilon\eta$ -2 η
$\vec{C}(l, 2) = \sqrt{\frac{2}{3}}$			0 η^* η^* η^* 0 η η η
$E_g : E/\Gamma = 19 - 3R$			
$\vec{C}(c, 3a) =$	-1 0 0 0 0 ϵ ϵ^* 1	$\vec{C}(c, 3b) =$	0 ϵ^* ϵ 1 -1 0 0 0

(Edmonds)] from which the $D_{m'm}^{2*}(h)$ are immediately obtained using Table II:

$$D_{m'm}^{2*}(\alpha\beta\gamma) = e^{im'\alpha} d_{m'm}(\beta) e^{im\gamma}. \quad (\text{A14})$$

The resulting values of

$$P_m = \sum_{\alpha, h} D_{m-\alpha}^{2*}(h) C_h^\alpha$$

for each of the modes is given in Table XII along with $\sum_m |P_m|^2$ and hence the powder averages of the Raman intensities. From Mertens *et al.*,⁷ $A = \frac{1}{18}(37 + 25\sqrt{3}i)$, so that $\cos^2(\chi/2) = 0.8248$ and the intensity ratios of the modes $E_g : T_g^{(1)} : T_g^{(2)}$ are $1 : \frac{1}{2} \cos^2 \frac{1}{2} \chi : \frac{1}{2} \sin^2 \frac{1}{2} \chi$ or $1 : 0.413 : 0.088$. These are the results given previously.⁸

The scattering matrices in the crystal cubic frame can be obtained using Eq. (4):

$$P_{XZ} = \langle 0 | \alpha_{XZ} | \vec{k}=0 \rangle / K = P_1 - P_{-1}, \quad (\text{A15})$$

etc. The results for the lower E_g mode are given in Table VIII. A simple linear combination of the P 's yields the following real matrices:

$$\frac{-i}{\sqrt{2}} \left(\underline{P}(c, 3a) + \underline{P}(c, 3b) \right) = \frac{8}{3} \begin{bmatrix} 1 & 0 & 0 \\ 0 & 1 & 0 \\ 0 & 0 & -2 \end{bmatrix},$$

$$\frac{1}{\sqrt{2}} \left(\underline{P}(c, 3a) - \underline{P}(c, 3b) \right) = \frac{8}{3} \begin{bmatrix} -\sqrt{3} & 0 & 0 \\ 0 & \sqrt{3} & 0 \\ 0 & 0 & 0 \end{bmatrix}.$$

In a similar way the scattering matrices for the two T_g modes can be put in the form

TABLE X. Sublattice directions and Euler angles for transforming from cubic to h frame.

Sublattice index	Direction of Z-axis	Direction of X-axis	Euler angles for taking cubic frame to h frame		
			α	β	γ
h					
0	[111]	[110]	$\frac{1}{4}\pi$	$\cos\beta = \frac{1}{3}$	$\frac{1}{2}\pi$
1	[111]	[011]	$\frac{3}{4}\pi$	$\cos\beta = \frac{1}{3}$	$\frac{5}{6}\pi$
2	[111]	[101]	$\frac{7}{4}\pi$	$\cos\beta = \frac{1}{3}$	$\frac{1}{6}\pi$
3	[111]	[110]	$\frac{1}{4}\pi$	$\cos\beta = -\frac{1}{3}$	$\frac{1}{2}\pi$

TABLE XI. $d_{m'm}^2(\beta) = (-1)^{m'} {}^{-m}d_{mm'}^2(\beta)$.

m'	m				
	+2	+1	0	-1	-2
+2	$\frac{1}{4}(1+\cos\beta)^2$				
+1	$\frac{1}{2}\sin\beta(1+\cos\beta)$	$\frac{1}{2}(\cos\beta+\cos 2\beta)$			
0	$(\sqrt{3}/2\sqrt{2})\sin^2\beta$	$(\sqrt{3}/2\sqrt{2})\sin 2\beta$	$\frac{1}{4}(1+3\cos 2\beta)$		
-1	$\frac{1}{2}\sin\beta(1-\cos\beta)$	$\frac{1}{2}(\cos\beta-\cos 2\beta)$	$(\sqrt{3}/2\sqrt{2})\sin 2\beta$	$\frac{1}{2}(\cos\beta+\cos 2\beta)$	
-2	$\frac{1}{4}(1-\cos\beta)^2$	$\frac{1}{2}\sin\beta(1-\cos\beta)$	$(\sqrt{3}/2\sqrt{2})\sin^2\beta$	$\frac{1}{2}\sin\beta(1+\cos\beta)$	$\frac{1}{4}(1+\cos\beta)^2$

$$\begin{bmatrix} 0 & 0 & 0 \\ 0 & 0 & M \\ 0 & M & 0 \end{bmatrix}, \begin{bmatrix} 0 & 0 & M \\ 0 & 0 & 0 \\ M & 0 & 0 \end{bmatrix}, \begin{bmatrix} 0 & M & 0 \\ M & 0 & 0 \\ 0 & 0 & 0 \end{bmatrix},$$

where $M = \frac{8}{3} \cos \frac{1}{2} \kappa$ for $T_g^{(1)}$ and $\frac{8}{3} \sin \frac{1}{2} \kappa$ for $T_g^{(2)}$. These are precisely the scattering tensors listed by Loudon⁵⁹ for the Raman-active vibrational modes of cubic crystals, class $m3(T_h)$ (the tensors for the E_g modes given in his table are in error and were later corrected). Such a correspondence is presumably required by group theory. It is a further demonstration of the very close similarity between the quantum-mechanical librations of $J=1$ molecular hydrogen and the classical librational modes of solids such as N_2 and CO_2 , first pointed out by ourselves^{8,11} and later demonstrated formally by Coll *et al.*¹³

The intensities for a single crystal have been obtained from Eq. (12) by inserting the appropriate Euler angles. For the present experiments in which one of the [111] body diagonals of the crystal is along the laboratory Z axis, the first two Euler angles correspond exactly to the α 's and β 's given in Table X. Choosing α and β to be that of sublattice $h=0$ and leaving γ (which represents a rotation about the [111] axis) as a variable, the quantities

$$D_m = \sum_{m'} D_{m'm}^2(c) P_{m'} \quad (A16)$$

are generated, where (c) denotes the just defined Euler angles. The results are given in Table XII. Finally, the scattering matrices in the laboratory frame are obtained:

TABLE XII. Values of P_m and D_m for Libron modes.

	E_g		Mode symmetry $l, 2$	$T_g^{(2)}$	
	$C, 3a$	$C, 3b$		$C, 2a$	
P_0^a	$-i6\sqrt{2}d$	$-i6\sqrt{2}d$	0	0	0
P_1	0	0	$4de^{-i\pi/4} \cos \frac{1}{2} \chi$	$(\sqrt{3}+1)de^{-i\pi/4}(1+\eta^*)$	P_1^*
P_{-1}	0	0	$4de^{i\pi/4} \cos \frac{1}{2} \chi$	$-\sqrt{3}-1)de^{i\pi/4}(1+\eta^*)$	P_1^*
P_2	$6d$	$-6d$	$-2\sqrt{2}d \cos \frac{1}{2} \chi$	$\sqrt{2}d(1+\eta^*)$	$-P_2^*$
P_{-2}	$6d$	$-6d$	$2\sqrt{2}d \cos \frac{1}{2} \chi$	$-\sqrt{2}d(1+\eta^*)$	$-P_2^*$
$\sum P_m ^2$	$\frac{32}{3}$	$\frac{32}{3}$	$a = \frac{32}{9} \cos^2 \frac{1}{2} \chi$	a	a
D_0	0	0	$\frac{4}{3}\sqrt{2} \cos \frac{1}{2} \chi$	0	0
D_1	$-i8/3e^{i\gamma}$	0	0	$i2d(1+\eta^*)e^{i\gamma}$	0
D_{-1}	0	D_1^*	0	0	D_1^*
D_2	$-\frac{1}{3}i4\sqrt{2}e^{-i2\gamma}$	0	0	$-i2\sqrt{2}d(1+\eta^*)e^{-i2\gamma}$	0
D_{-2}	0	$-D_2^*$	0	0	$-D_2^*$
$\sum D_m ^2$	$\frac{32}{3}$	$\frac{32}{3}$	$a = \frac{32}{9} \cos^2 \frac{1}{3} \chi$	a	a

^a $\eta = e^{i\chi} = A/|A|$; $d = \sqrt{2}/3\sqrt{3}$; $|1-\eta^*|^2 = 4 \sin^2 \frac{1}{2} \chi$; $|1+\eta^*|^2 = 4 \cos^2 \frac{1}{2} \chi$; Results for $(l, 1)$ mode are obtained by replacing $\cos \frac{1}{2} \chi$ in $(l, 2)$ mode with $-i \sin \frac{1}{2} \chi$. Similarly, $(1+\eta^*)$ in $(C, 2a)$ mode is replaced with $(1-\eta^*)$ to obtain results for $(C, 1a)$ mode.

TABLE XIII. Elements of scattering matrices for E_g mode.

Mode	(C, 3a)	(C, 3b)
P_{XX}	$\frac{4}{3}\sqrt{2}(i+\sqrt{3})$	$\frac{4}{3}\sqrt{2}(i-\sqrt{3})$
P_{YY}	$\frac{4}{3}\sqrt{2}(i-\sqrt{3})$	$\frac{4}{3}\sqrt{2}(i+\sqrt{3})$
P_{ZZ}	$-\frac{8}{3}\sqrt{2}i$	$-\frac{8}{3}\sqrt{2}i$
$P_{XY}=P_{XZ}=P_{YZ}=0$		$P_{XY}=P_{XZ}=P_{YZ}=0$

$$D_{XZ} = \langle 0 | \alpha_{XZ} | \vec{k} = 0 \rangle / K = D_1 - D_{-1}, \quad (\text{A17})$$

etc. The $D_{\sigma\rho}$ depend only on γ as $e^{i\gamma}$ or $e^{i2\gamma}$ and therefore the intensities, proportional to $|D_{\sigma\rho}|^2$, will be independent of γ .

APPENDIX B: LINEAR COMBINATIONS OF $J=1 \rightarrow 3$ RAMAN SPECTRA

In order to subtract one $J=1 \rightarrow 3$ spectrum from another it was necessary to convert the spectra to a common frequency scale. The first step was to very carefully digitize the spectra along with their respective frequency marker traces by direct measurements of the original strip-chart recordings. This was done using an X-Y recorder with a sharp point in place of the writing pen: The X-axis voltage was stepped uniformly while the Y-axis voltage was adjusted to follow the trace. Both voltages were digitized and recorded on paper tape, and then transferred to IBM cards. The next step was to smooth the periodic marker traces so that they could be used for interpolation of the spectrometer frequency. The smoothing was necessary not only to reduce the noise on the marker trace but also to remove the higher harmonics from the periodic wave form which, due to the nature of the Fabry-Perot etalon, is not a pure sine wave. Since the period of the markers was not a constant (the spectrometer drive was not uniform in time), one could not use a filtering function that was sharply peaked at

some fixed frequency. This would have the effect of shifting the true maxima and minima of the marker whenever the marker frequency varied from the filter frequency. We chose the weighting function in frequency space to be $\sin^2(\pi f/2f_0)$ for $0 < f < 2f_0$ and zero elsewhere (f_0 is the average frequency of the marker wave form).

This weighting function is zero at $f=0$ and at all harmonics of the average frequency f_0 , yet is not sharply peaked at f_0 and will allow minor changes in frequency with very little distortion. Now, if the filtering were applied directly to the finite wave forms (which typically included only 12 complete cycles), the disturbances produced by discontinuities at the end points would be substantial. We therefore artificially enlarged the traces by reflecting the marker traces about carefully chosen end points, and in addition tapered these added sections to zero at the leading and trailing ends. Smoothing of this wave form then resulted in something very close to a sine wave which had almost no discernible noise and for which the peaks corresponded extremely well with the peaks of the original marker trace. Interpolation was then accomplished by assuming each peak and the following valley to be a sinusoid of constant amplitude (but possibly changing frequency). In this way each of the $J=1 \rightarrow 3$ Raman spectra was converted to a common frequency scale. Linear combinations of the spectra could then easily be computed and plotted.

Note added in proof. The authors have just learned [T. Nakamura (private communication)] that the $J=3$ perturbations on the libron frequencies given in Ref. 30 are in error. They should read -53 , -39 , and -27 instead of -53 , -20 , and -61 (units of Γ^2/B). Together with shifts 81, 66, and 48 due to polarization of the ground state, the final results are 28, 27, and 21 Γ^2/B . This gives values of Γ_{eff} for the respective modes of 0.765, 0.768, and 0.771 cm^{-1} for D_2 and 0.584, 0.598, and 0.597 cm^{-1} for H_2 .

*Alfred P. Sloan Foundation Fellow.

†Present address.

‡Contribution No. 3162.

¹The analogy between hydrogen and magnetic systems has been discussed in some detail by A. B. Harris [J. Appl. Phys. **42**, 1574 (1971)]. This paper and the article by I. F. Silvera [Proceedings of the International School of Physics Enrico Fermi, Varenna, Course LVI (1972) (unpublished)] are also useful as general reviews on solid hydrogen.

²R. L. Mills, J. L. Yarnell, and A. F. Schuch, in *Proceedings of the Thirteenth International Conference of*

Low-Temperature Physics, edited by W. J. O'Sullivan, K. D. Timmerhaus, and E. F. Hammel (Plenum, New York, 1974).

³A. F. Schuch, R. L. Mills, and D. A. Depatie, Phys. Rev. **165**, 1032 (1968).

⁴K. F. Mucker, P. M. Harris, D. White, and R. A. Erickson, J. Chem. Phys. **49**, 1922 (1968).

⁵J. Felsteiner, Phys. Rev. Lett. **15**, 1025 (1965); J. C. Raich and H. M. James, Phys. Rev. Lett. **16**, 173 (1966); H. M. James and J. C. Raich Phys. Rev. **162**, 647 (1967).

⁶S. Homma, K. Okada, and H. Matsuda, Prog. Theor.

- Phys. 36, 1310 (1966); 38, 767 (1967); 45, 330 (1971) (erratum); H. Ueyama and T. Matsubara, *ibid.* 36, 784 (1967); J. C. Raich and R. E. Etters, Phys. Rev. 168, 425 (1968).
- ⁷F. G. Mertens, W. Biem, and H. Hahn, Z. Phys. 213, 33 (1968).
- ⁸W. N. Hardy, I. F. Silvera, and J. P. McTague, Phys. Rev. Lett. 22, 297 (1969).
- ⁹A. J. Berlinsky, A. B. Harris, and C. F. Coll, III, Solid State Commun. 7, 1491 (1969).
- ¹⁰A. B. Harris, Phys. Rev. B 1, 1881 (1970).
- ¹¹I. F. Silvera, W. N. Hardy, and J. P. McTague, Disc. Faraday Soc. 48, 54 (1969).
- ¹²H. M. James, Phys. Rev. B 2, 2213 (1970); Phys. Rev. Lett. 24, 815 (1970); 24, 970(E) (1970). Note that the $P4_2/mnm$ ordering was inadvertently mislabeled $Cmmm$ in the first article.
- ¹³C. F. Coll, III and A. B. Harris, Phys. Rev. B 2, 1176 (1970).
- ¹⁴T. Nakamura and H. Miyagi, Prog. Theor. Phys. 44, 833 (1970).
- ¹⁵C. F. Coll, III, A. B. Harris, and A. J. Berlinsky, Phys. Rev. Lett. 25, 858 (1970).
- ¹⁶C. F. Coll, III and A. B. Harris, Phys. Rev. B 4, 2781 (1971).
- ¹⁷A. J. Berlinsky and A. B. Harris, Phys. Rev. B 4, 2808 (1971).
- ¹⁸W. N. Hardy, I. F. Silvera, and J. P. McTague, Phys. Rev. Lett. 26, 127 (1971).
- ¹⁹A. B. Harris, A. J. Berlinsky, and H. Meyer, Phys. Rev. B 7, 4720 (1973).
- ²⁰D. Ramm, H. Meyer, and J. F. Jarvis, Solid State Commun. 6, 497 (1968); J. F. Jarvis, H. Meyer, and D. Ramm, Phys. Rev. 178, 1461 (1969); D. Ramm, H. Meyer, and R. L. Mills, Phys. Rev. B 1, 2763 (1970).
- ²¹H. Meyer, F. Weinhaus, and B. Maraviglia, Phys. Rev. B 6, 1112 (1972); see also B. Maraviglia, F. Weinhaus, H. Meyer, and R. L. Mills, Solid State Commun. 8, 815 (1970); 8, 1683 (1970).
- ²²H. Stein, H. Stiller, and R. Stockmeyer, J. Chem. Phys. 57, 1726 (1972). A thorough reanalysis of this experimental work is given by A. B. Harris and A. J. Berlinsky (unpublished).
- ²³M. J. Clouter, H. P. Gush, and H. L. Welsh, Can. J. Phys. 48, 237 (1970); a preliminary report of these results can be found in a theoretical paper by S. Homma and H. Matsuda [Prog. Theor. Phys. 40, 1191 (1968)].
- ²⁴I. F. Silvera, W. N. Hardy and J. P. McTague, Rev. Sci. Instr. 43, 58 (1972).
- ²⁵D. A. Depatie and R. L. Mills, Rev. Sci. Instr. 39, 105 (1968).
- ²⁶By a mass-spectrometer analysis of several of the gaseous samples, the level of nonhydrogen impurities was estimated to be well below 0.01%. The only impurities that could have appreciable partial pressures at the solidification temperature of H_2 and D_2 are helium and neon. From the work of W. B. Street, R. E. Sonntag, and G. J. Van Wylen [J. Chem. Phys. 40, 1390 (1964)], the solubility of 4He in liquid normal H_2 at 17 K is about 2×10^{-4} mole%/Torr of helium pressure in the gas; the solubility will be considerably less in the solid at the melting point, and will further decrease as the temperature is lowered. The solubility of neon is similarly low.
- ²⁷J. P. McTague, I. F. Silvera, and W. N. Hardy, Bull. Am. Phys. Soc. 15, 296 (1970); and I. F. Silvera, W. N. Hardy, and J. P. McTague, Phys. Rev. B 4, 1578 (1972).
- ²⁸A puzzling feature of our experiments was the consistently lower signal-to-noise ratio observed in hydrogen. Although quantitative measurements were not made, the effect did not seem to be accounted for by the differences in density and in anisotropy of the polarizability.
- ²⁹T. Nakamura and H. Miyagi, Prog. Theor. Phys. 44, 833 (1970); see also 44, 1430 (1970) (erratum).
- ³⁰T. Nakamura, H. Miyagi, and M. Fujio, in *Proceedings of the Twelfth International Conference of Low-Temperature Physics*, edited by Eizo Kanda (Academic of Japan, Kyoto, 1970); M. Fujio and T. Nakamura (private communication).
- ³¹A. J. Berlinsky, Ph.D. thesis (University of Pennsylvania, 1972) (unpublished); and private communication.
- ³²This procedure was adopted by Meyer and co-workers in their NMR studies of the ordered phase. It is based on the result of A. F. Schuch, R. L. Mills, and D. A. Depatie [Phys. Rev. 165, 1032 (1968)] that thermal cycling through the transition temperature stabilizes the fcc structure over the hcp phase and an unidentified intermediate structure, so that one can pass through the orientational transition while remaining in the cubic phase.
- ³³J. P. McTague, W. N. Hardy, and I. F. Silvera (unpublished).
- ³⁴J. C. Raich (private communication).
- ³⁵R. J. Lee and J. C. Raich, Phys. Rev. Lett. 27, 1137 (1971). There is a misprint in this paper and $\bar{n} = \frac{1}{3}(1 + \frac{1}{2} \langle \theta^2 \rangle)$ rather than $\bar{n} = \frac{1}{2}(1 + \frac{1}{3} \langle \theta^2 \rangle)$, so that $(1 - \frac{3}{2} J_z^2) = 1 - 3\bar{n}$. A table of \bar{n} vs T was supplied by J. C. Raich.
- ³⁶W. N. Hardy and A. J. Berlinsky, Phys. Rev. B 8, 4996 (1973).
- ³⁷A. J. Berlinsky and C. F. Coll, III, Phys. Rev. B 5, 1587 (1972).
- ³⁸Values of the quantity
- $$\operatorname{Re} W(x + iy) = \frac{1}{\pi} \int_{-\infty}^{+\infty} \frac{ye^{-t^2}}{y^2 + (x-t)^2} dt$$
- are given in Handbook of Mathematical Functions [edited by M. Abramowitz and I. A. Stegun (Dover, New York, 1965), pp. 302 and 325].
- ³⁹W. R. C. Prior, Ph.D. thesis (University of Toronto, 1971) (unpublished).
- ⁴⁰M. J. Clouter, H. P. Gush, and H. L. Welsh, Can. J. Phys. 48, 237 (1970).
- ⁴¹J. Van Kranendonk, Can. J. Phys. 38, 240 (1960).
- ⁴²J. P. McTague, I. F. Silvera, and W. N. Hardy, *Proceedings of the Second International Conference on Light Scattering in Solids*, edited by M. Balkanski (Flammarion Sciences, New York, 1971), p. 456.
- ⁴³S. S. Bhatnagar, E. J. Allin, and H. L. Welsh, Can. J. Phys. 40, 9 (1962).
- ⁴⁴J. C. Raich and H. M. James, Phys. Rev. 162, 649 (1967).
- ⁴⁵S. A. Boggs, M. J. Clouter, and H. L. Welsh, Can. J. Phys. 50, 2063 (1972).
- ⁴⁶I. F. Silvera, W. N. Hardy, and J. P. McTague, Phys.

Rev. B 5, 1578 (1972).

⁴⁷R. J. Lee, J. C. Raich, and R. D. Etters, J. Low Temp. Phys. 2, 255 (1970).

⁴⁸A. J. Berlinsky and W. N. Hardy (unpublished).

⁴⁹A. J. Berlinsky and A. B. Harris, Phys. Rev. A 1, 878 (1970).

⁵⁰J. F. Jarvis, H. Meyer, and D. Ramm, Phys. Rev. 178, 1461 (1969).

⁵¹This unpublished data comes from the NMR work of F. Weinhaus *et al.* [Phys. Rev. 33, 626 (1971)], and was communicated privately to us by R. F. Buzerak.

⁵²G. Grenier and D. White, J. Chem. Phys. 40, 3015 (1964).

⁵³A. J. Berlinsky and W. N. Hardy (unpublished).

⁵⁴It may be possible to reduce the conversion rate in para-D₂ by pressurizing the sample sufficiently to reduce the density of phonon final states required in the

conversion process.

⁵⁵H. Meyer (private communication).

⁵⁶J. Van Kranendonk and G. Karl, Rev. Mod. Phys. 40, 531 (1968).

⁵⁷E. B. Wilson, J. C. Decius, and P. C. Cross, *Molecular Vibrations* (McGraw-Hill, New York, 1955), p. 48.

⁵⁸M. Born and K. Huang, *Dynamical Theory of Crystal Lattices* (Clarendon, Oxford, 1954).

⁵⁹R. Loudon, Adv. Phys. 13, 423 (1964); see also Errata, 14, 621 (1965) (errata).

⁶⁰A. R. Edmonds, *Angular Momentum in Quantum Mechanics* (Princeton U. P., Princeton, 1960).

⁶¹Throughout this paper the conventions for spherical harmonics and rotation matrices will be those of M. E. Rose [*Elementary Theory of Angular Momentum* (Wiley, New York, 1957)].